# Cohesin loss alters adult hematopoietic stem cell homeostasis, leading to myeloproliferative neoplasms

Jasper Mullenders,[1,2] Beatriz Aranda-Orgilles,[1,2] Priscillia Lhoumaud,[2] Matthew Keller,[1,2] Juhee Pae,[1,2] Kun Wang,[1,2] Clarisse Kayembe,[1,2] Pedro P. Rocha,[2] Ramya Raviram,[2] Yixiao Gong,[1,2] Prem K. Premsrirut,[5] Aristotelis Tsirigos,[2,3] Richard Bonneau,[4] Jane A. Skok,[2] Luisa Cimmino,[1,2] Daniela Hoehn,[6] and Iannis Aifantis[1,2]

[1]Howard Hughes Medical Institute, [2]Department of Pathology, and [3]Center for Health Informatics and Bioinformatics, School of Medicine and [4]Department of Biology, Center for Genomics and Systems Biology, New York University, New York, NY 10016
[5]Mirimus Inc., Woodbury, NY 11797
[6]Department of Pathology and Cell Biology, Columbia University Medical Center, New York, NY 10032

**The cohesin complex (consisting of Rad21, Smc1a, Smc3, and Stag2 proteins) is critically important for proper sister chromatid separation during mitosis. Mutations in the cohesin complex were recently identified in a variety of human malignancies including acute myeloid leukemia (AML). To address the potential tumor-suppressive function of cohesin in vivo, we generated a series of shRNA mouse models in which endogenous cohesin can be silenced inducibly. Notably, silencing of cohesin complex members did not have a deleterious effect on cell viability. Furthermore, knockdown of cohesin led to gain of replating capacity of mouse hematopoietic progenitor cells. However, cohesin silencing in vivo rapidly altered stem cells homeostasis and myelopoiesis. Likewise, we found widespread changes in chromatin accessibility and expression of genes involved in myelomonocytic maturation and differentiation. Finally, aged cohesin knockdown mice developed a clinical picture closely resembling myeloproliferative disorders/neoplasms (MPNs), including varying degrees of extramedullary hematopoiesis (myeloid metaplasia) and splenomegaly. Our results represent the first successful demonstration of a tumor suppressor function for the cohesin complex, while also confirming that cohesin mutations occur as an early event in leukemogenesis, facilitating the potential development of a myeloid malignancy.**

CORRESPONDENCE
Iannis Aifantis:
Iannis.Aifantis@nyumc.org

Abbreviations used: AML, acute myeloid leukemia; ES, embryonic stem; FC, fold change; GMP, granulocyte-macrophage progenitor; GSEA, gene set enrichment analysis; HSC, hematopoietic stem cell; LT-HSC, long-term HSC; MPN, myeloproliferative neoplasm; MPP, multipotent progenitor; qRT-PCR, quantitative real-time PCR; rtTA, reverse tTA; SCC, sister chromatid cohesion; Tet, tetracycline; TRE, Tet-responsive element; tTA, Tet transcriptional activator; UTR, untranslated region.

Cohesin is a multimeric protein complex that is very well conserved throughout evolution and across species and is critically important in mediating proper sister chromatid cohesion (SCC) and separation from S phase to M phase during mitosis (Hirano, 2005; Nasmyth and Haering, 2009). The complex consists of four proteins Rad21, Smc1a, Smc3, and Stag2 (also known as SA-2) that form a ring structure that can physically wrap around the chromatin (Gruber et al., 2003). During the different phases of cell division, additional regulator proteins (e.g., NIPBL, HDAC8, and WAPL) are required for its proper function (Haarhuis et al., 2014). Cohesin's ring structure is also essential for its additional functions, namely DNA repair and three-dimensional chromatin looping. The latter has been studied extensively in embryonic stem (ES) cells where cohesin controls core pluripotency genes by assisting the looping of enhancers to specific promoters (Kagey et al., 2010). Genome-wide studies have shown that cohesin predominantly co-occurs with CTCF on the chromatin of mammalian cells (Parelho et al., 2008; Wendt et al., 2008). Sites that are bound by both CTCF and cohesin were proposed to serve as anchoring points for long-range genomic interactions (Dowen et al., 2014), suggesting that cohesin together with CTCF dictates higher-order chromatin structure (Holwerda and de Laat, 2012). For instance, in ES cells it



The Rockefeller University Press $30.00
J. Exp. Med. 2015 Vol. 212 No. 11 1833–1850
www.jem.org/cgi/doi/10.1084/jem.20151323

was shown that CTCF and cohesin help to establish borders of topologically associated domains (TADs), and these structures have been shown to play a major role in delimiting regulatory interactions (Dixon et al., 2012; Phillips-Cremins et al., 2013; Dowen et al., 2014). Not surprisingly, suppression of cohesin leads to unfolding and relaxation of topological domains (Sofueva et al., 2013; Mizuguchi et al., 2014). This implies that cohesin is an important regulator of transcription through genome-wide chromatin organization. Another way that cohesin regulates transcription is by acting as a docking site for transcription factors in cells that exit mitosis. Cohesin is one of the last protein complexes to leave the condensing chromatin in mitosis, serving as a cellular memory for transcription factors to bind postmitotically (Yan et al., 2013).

Large-scale sequencing studies have identified mutations in the cohesin complex (Rad21, SCM1A, Smc3, Stag2, and NIPBL) in a variety of human malignancies, and its association with myeloid malignancies is particularly striking (Huether et al., 2014; Leiserson et al., 2015). Notably recurrent mutations have been observed in acute myeloid leukemia (AML) cases de novo AML and AML with myelodysplasia-related changes (10–20%), down syndrome–associated acute megakaryoblastic leukemia (50% DS-AMKL), myelodysplastic syndromes (5–15%), and myeloproliferative neoplasms (MPNs; up to 10%), as classified according to the 2008 WHO classification for hematopoietic and lymphoid tissue (Ding et al., 2012; Cancer Genome Atlas Research Network, 2013; Kon et al., 2013; Nikolaev et al., 2013; Yoshida et al., 2013; Thol et al., 2014; Thota et al., 2014; Lindsley et al., 2015). In addition, somatic mutations have been found in a wide range of solid cancers like bladder cancer (20%) and Ewing's sarcoma (20%; Balbás-Martínez et al., 2013; Guo et al., 2013; Solomon et al., 2013; Crompton et al., 2014; Tirode et al., 2014). Besides the aforementioned somatic mutations, germline mutations of cohesin have been described in patients with developmental syndromes, particularly Cornelia de Lange syndrome (CdLS; Mannini et al., 2013).

In general, mutations in different members of the cohesin complex appear to be mutually exclusive, suggesting that these proteins are not functionally redundant (Leiserson et al., 2015). Mutations in cohesin predominantly fall into two categories: in *Rad21* and *Stag2* genes many truncations and frame-shift mutations are found, whereas in *Smc1a* and *Smc3* genes mostly missense mutations are observed (Kon et al., 2013). In addition, genomic deletions for *Rad21* and *Stag2* are also identified in several tumor types (Rocquain et al., 2010; Solomon et al., 2011). The genes coding for *Smc1a* and *Stag2* are located on chromosome X, and as such, mutations in *Smc1a* and *Stag2* are expected to have a stronger impact, as there is no wild-type copy present in tumors (Solomon et al., 2011).

All mutations rather appear to cause reduced or altered function, as a complete loss of function of any of the core components of cohesin has proven to be incompatible with cellular proliferation and survival, as a result of their essential role in SCC (Xu et al., 2010). For example, homozygous knockout mouse models for cohesin exhibit early embryonic lethality, therefore limiting comprehensive investigations of cohesin in vivo (Xu et al., 2010; Seitan et al., 2011). In this study, we present the first successful in vivo loss of function murine models for distinct cohesin members. We have created RNAi mouse models that inducibly knock down Rad21, Smc1a, and Stag2 systemically.

We observed that induction of the shRNA in vivo resulted in an ∼80% loss of mRNA/protein expression that strikingly did not lead to adverse effects on proliferation. Moreover, cohesin knockdown leads to a shift in the hematopoietic stem compartment and increases the replating capacity of these cells. Over time, cohesin knockdown mice developed clinical features of myeloproliferative disorders/neoplasms. We did not observe genomic instability in cohesin knockdown cells, suggesting that these phenotypes are caused by misregulation of cohesin's role on gene expression and genome organization. These findings provide the first in vivo evidence that cohesin governs adult stem cell homeostasis and myeloid development, potentially functioning as tumor suppressor in the hematopoietic system.

## RESULTS

### AML-derived cohesin mutations can impair core complex formation

To determine the effect of mutations found in AML patients on cohesin complex formation, we initially modeled selected mutations in vitro. We overexpressed wild-type and AML mutant cohesin proteins in 293T cells and used immunoprecipitation to pull down the endogenous cohesin complex. As expected, all wild-type cohesin proteins strongly interact with the other members of the core complex. Strikingly, several AML-derived mutations completely abrogated complex formation. This is most clear in the case of Rad21 (Fig. 1 A) and Stag2 (Fig. 1 B). The underlying reasons why these proteins no longer interact with the other members of the complex could be diverse; in the case of Rad21, the short fragments appear to be unstable (Zhang et al., 2013). For Stag2, the C terminus of the protein has been reported to be important for protein function as it is the location of many phosphorylation sites and potentially the nuclear localization signal (Hauf et al., 2005; Solomon et al., 2011). Truncation of Stag2 will hence cause loss of the phosphorylation and potential loss of nuclear localization. For Smc3, we noticed that one mutation (R245*) causes complete loss of complex formation (Fig. 1 C) and a milder phenotype for some of the other mutations.

### Cohesin silencing leads to increased replating capacity in vitro

We have shown that many recurrent cohesin mutations found in AML patients are likely to result in loss of function of the protein involved (Fig. 1). This is supported by large-scale sequencing efforts in AML samples (Kon et al., 2013), suggesting such a function for cohesin mutations. For this reason, we chose an RNAi-mediated knockdown strategy to suppress endogenous cohesin proteins. We created between five and nine retroviral shRNA vectors for each of the cohesin core

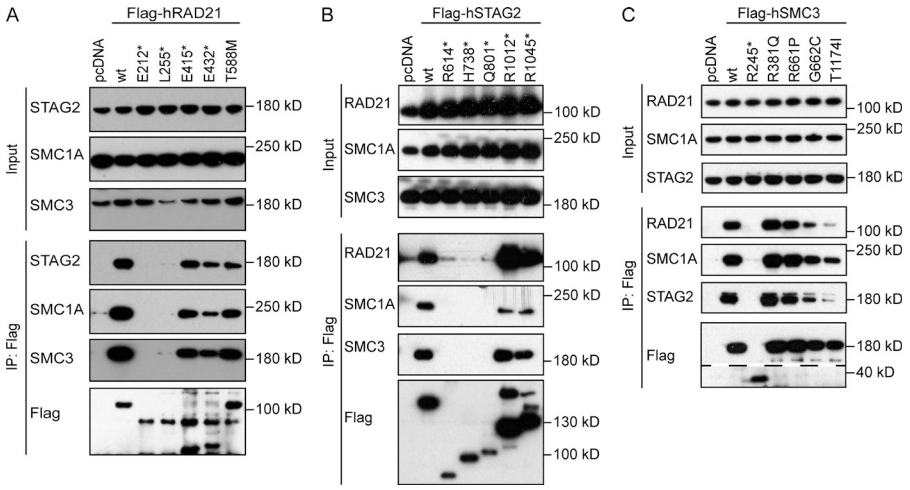


**Figure 1. Cohesin mutations in AML cause loss of function and disrupt core complex formation.** (A) Flag-tagged wild-type and AML patient mutants of Rad21 were transfected in 293T cells. After immunoprecipitation with Flag-beads, Western blot analysis was performed for endogenous Smc1a, Smc3, and Stag2 protein. Some Rad21 fragments (E212* and L255*) are poorly expressed, possibly because of degradation (Zhang et al., 2013). (B) Flag-tagged wild-type and AML patient mutants of Stag2 were transfected in 293T cells. After immunoprecipitation with Flag-beads, Western blot analysis was performed for endogenous Rad21, Smc1a, and Smc3 protein. Stag2 mutants R614* and H738* are known to be aberrantly localized to the cytoplasm; this is possibly the case for Q801* as well (Solomon et al., 2011). (C) Flag-tagged wild-type and AML patient mutants of Smc3 were transfected in 293T cells. After immunoprecipitation with Flag-beads, Western blot analysis was performed for endogenous Rad21, Smc1a, and Stag2 protein. Dashed line indicates intervening lanes were spliced out.

complex genes: *Rad21*, *Smc1a*, *Smc3*, and *Stag2* (Table S1). We chose a vector that expresses GFP in combination with the shRNA, enabling us to track cells expressing the shRNA. After cloning, these vectors were tested for their knockdown efficiency (not depicted). We selected two shRNA vectors for each *Rad21*, *Smc1a*, *Smc3*, and *Stag2* gene that suppressed the endogenous mRNA efficiently but not completely (75–90%), as we expected that a complete knockdown would be detrimental to the cells. First, we investigated what the effect of cohesin knockdown is on hematopoietic stem and progenitor cells. Therefore, we transduced mouse bone marrow c-Kit$^+$ hematopoietic progenitor cells with retroviral shRNA vectors for *Rad21*, *Smc1a*, *Smc3*, and *Stag2*. The infected cells were plated in methylcellulose for CFU assays (Fig. 2 A). Although control infected cells (shRNA targeting Renilla) yielded colonies for only two rounds of plating, all cohesin knockdown cells continued forming colonies after at least five rounds of plating in methylcellulose. This phenotype was reproducible and was validated using multiple independent shRNAs for the cohesin subunits (not depicted). Furthermore, the selected cells proliferated in liquid culture for prolonged periods of time (not depicted). We confirmed by quantitative real-time PCR (qRT-PCR) that shRNA-infected cells indeed demonstrated a strong reduction of endogenous cohesin transcripts (Fig. 2 B). Cohesin knockdown demonstrated decreased expression of the differentiation markers Cd11b and Gr1 (Fig. 2 C). This finding was coupled with increased c-Kit and Sca-1 expression as early as the first plating (Fig. 2 D).

Microscopically, we observed progressing cytomorphologic changes in the CFU assays. After several rounds of plating in methylcellulose, the cohesin knockdown cell population demonstrated a left shift in myelopoiesis, including a mild increase in mast cells, basophils, and eosinophils. The precursor cells exhibited slightly abnormal granulation, including lucent primary granules in conjunction with variable amounts of azurophilic/orangeophilic granules, whereas the more mature elements demonstrated a decrease in secondary granules. Mild nuclear cytoplasmic asynchrony as well as occasional myeloid/monocytoid elements with cytoplasmic vacuolization were also noted, compatible with GCSF effect from the culture medium (Fig. 2 E).

To gain a better understanding of the underlying changes in gene expression changes, we performed RNA sequencing of cells obtained from the first and fifth plating in methylcellulose (Fig. 2 F and Table S2). In agreement with protein expression data and the cellular phenotypes reported, we observed higher expression of c-Kit and Sca1 mRNA in cohesin knockdown cells compared with Renilla control cells. In addition, we observed that knockdown of all four cohesin members of the cohesin complex (Rad21, Smc1a, Smc3, and Stag2) resulted in comparable changes in gene expression, as is to be expected of members of such a nonredundant complex with presumably similar function (Fig. 2 F).

Although a prior study confirmed that cohesin gene mutant AML samples are largely cytogenetically normal (Cancer Genome Atlas Research Network, 2013), we wanted to rule out that cohesin knockdown causes severe effects in proper sister chromatid separation, leading to genomic instability. We thus analyzed metaphase spreads from cells from the first plating in methylcellulose and observed some metaphase spreads that showed typical loss of SCC (Fig. 2 G). Next, we quantified the number of metaphases that demonstrate this loss of SCC phenotype, which appeared to be a minority of cells in the culture (<15%; Fig. 2 H). This was not surprising as the majority of the cells were actively cycling and we did not observe massive cell death (not depicted). Moreover, we noticed that the loss of SCC phenotype seems to be counterselected over time (not depicted). These observations could explain the absence of any significant karyotype changes in cells that were obtained from the first methylcellulose plating (in the course of the experiment, these cells were proliferating

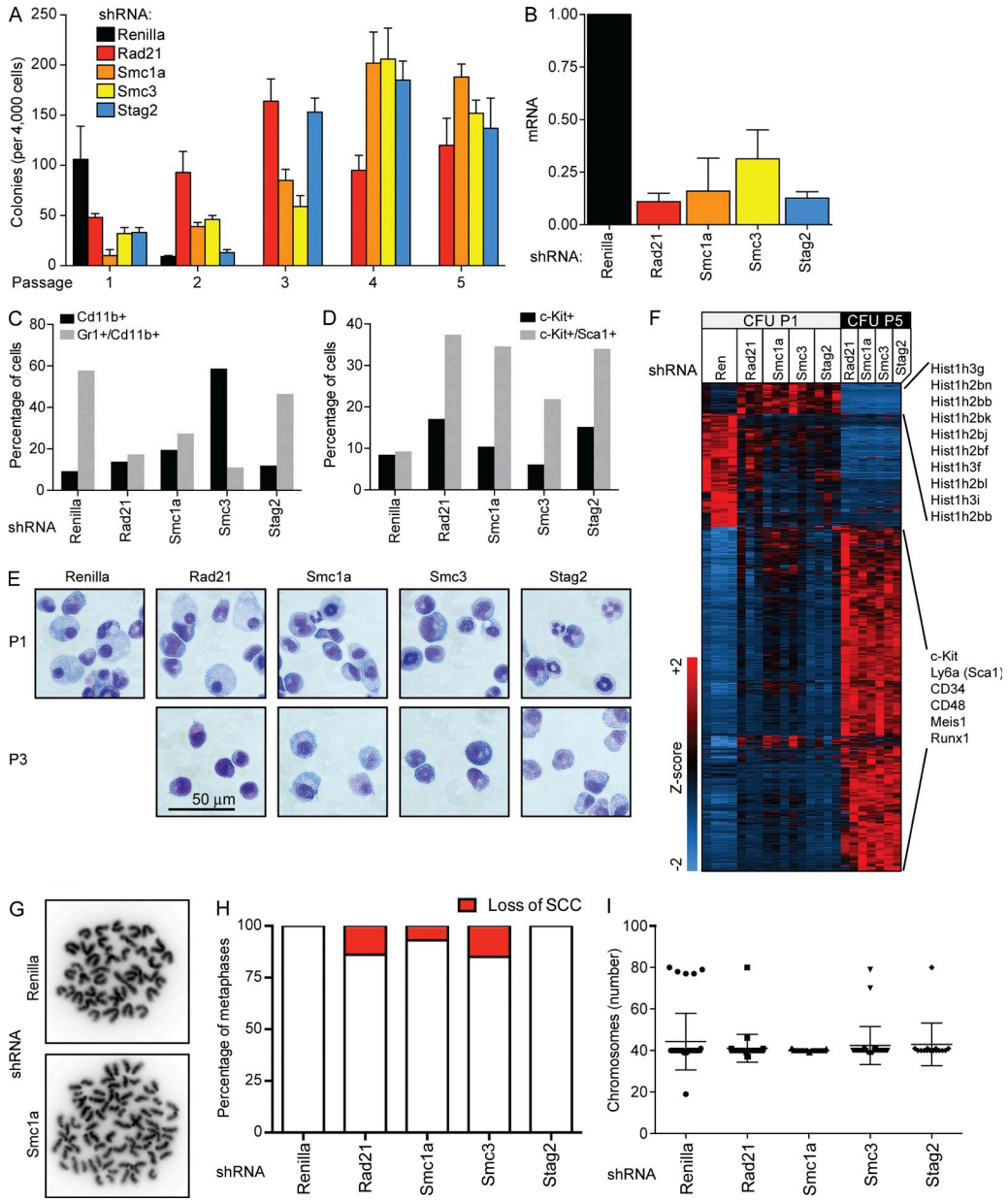


**Figure 2. Cohesin knockdown cells acquire replating capacity in vitro.** (A) Mouse c-Kit$^+$ cells were infected with retroviral shRNA vectors targeting Rad21, Smc1a, Smc3, and Stag2. Infected cells were seeded in methylcellulose and replated for five passages. (B) qRT-PCR to assess knockdown of Rad21, Smc1a, Smc3, and Stag2 shRNA–infected cells after the first plating in methylcellulose. (C and D) Quantification of flow cytometry analysis of Smc1a knockdown cells after the first (P1) and fourth plating (P4). Cells were stained for myeloid differentiation markers (Cd11b and Gr1; C) and stem cells markers c-Kit and Sca1 (D). (E) Morphology of Renilla and cohesin knockdown cells (as indicated) after the first and third plating in methylcellulose. (F) RNA-seq analysis of cohesin knockdown cells after the first (CFU P1) and fifth (CFU P5) plating in methylcellulose. Heat map shows genes that are significantly differently expressed ($P < 0.05$). (G) Metaphase spreads of control and Smc1a knockdown cells after the first plating in methylcellulose. (H) Quantification of fraction of metaphases that show loss of SCC in control and cohesin knockdown cells after the first plating in methylcellulose. (I) Quantification of number of chromosomes as counted in metaphase spreads of control and cohesin knockdown cells after the first plating in methylcellulose. Error bars indicate SD.

for ~14 d; Fig. 2 I). Overall, these studies suggest that not only hematopoietic stem and progenitor cells could survive when the expression of distinct cohesin members was significantly (but not totally) reduced, yet these same cells appeared to acquire the ability to self-renew in vitro. Such de novo replating capacity is frequently reported when putative AML tumor suppressors have been altered or silenced (Lee et al., 2007; Moran-Crusio et al., 2011; Quivoron et al., 2011).

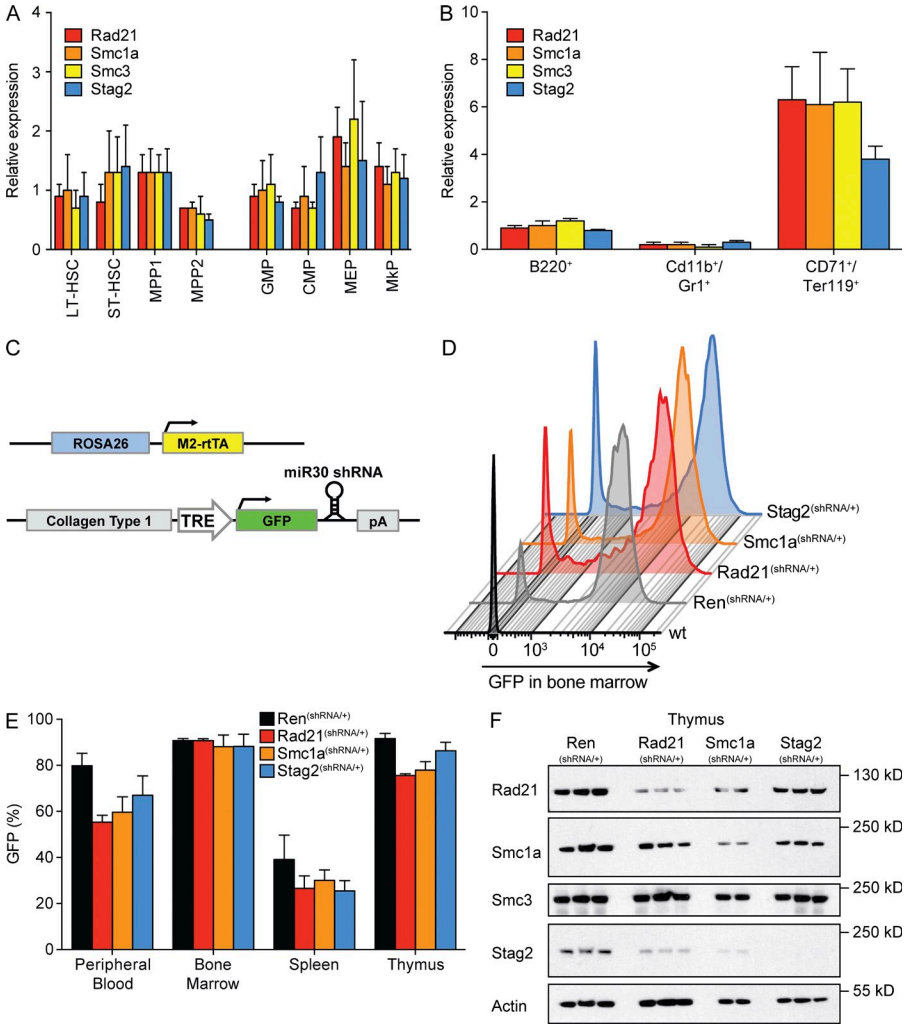


**Figure 3. Creation of mouse models for in vivo cohesin loss of function.** (A) qRT-PCR for cohesin core subunits (Rad21, Smc1a, Smc3, and Stag2) in the stem cell and progenitor compartment of mouse bone marrow. Cells were sorted as follows: LT-HSC ($Lin^-/c\text{-}Kit^+/Sca1^+/CD150^+$), short-term HSC (ST-HSC; $Lin^-/c\text{-}Kit^+/Sca1^+/CD48^-/CD150^-$), MPP1 ($Lin^-/c\text{-}Kit^+/Sca1^+/CD48^+/CD150^+$), MPP2 ($Lin^-/c\text{-}Kit^+/Sca1^+/CD48^+/CD150^-$), GMP ($Lin^-/c\text{-}Kit^+/Sca1^-/FcRII/III^+/CD34^+$), common myeloid progenitor (CMP; $Lin^-/c\text{-}Kit^+/Sca1^-/FcRII/III^-/CD34^+$), megakaryocyte-erythrocyte progenitor (MEP; $Lin^-/c\text{-}Kit^+/Sca1^-/FcRII/III^-/CD34^-$), and megakaryocyte progenitor (MkP; $Lin^-/c\text{-}Kit^+/Sca1^-/CD150^+/CD41^+$). (B) qRT-PCR for the cohesin subunits in bone marrow myeloid, erythroid, and B cells ($n = 3$). Cells were sorted from mouse bone marrow as follows: B cells ($B220^+$), myeloid cells ($Cd11b^+/Gr1^+$), and erythroblasts ($CD71^+/Ter119^+$). RNA was extracted and qRT-PCR performed for the indicated genes. (C) Schematic of loci used in an shRNA mouse. The ROSA26 locus drives constitutive expression of an M2rtTA transgene. Upon addition of doxycycline, the TRE in the Col1a1 locus is activated, which leads to expression of the shRNA, which is located in the 3′ UTR of GFP. (D) GFP expression after 10 d of doxycycline exposure in mouse total bone marrow of the indicated genotypes as measured by flow cytometry. (E) Mean frequency of GFP-expressing cells as measured by flow cytometry in the organs indicated. (F) Western blot analysis of total thymocytes from two to three individual animals (treated with doxycycline for 10 d) per genotype ($Ren^{(shRNA/+)}$, $Rad21^{(shRNA/+)}$, $Smc1a^{(shRNA/+)}$, and $Stag2^{(shRNA/+)}$). Error bars indicate SD.

## Generation of in vivo loss of function cohesin animal models

Encouraged by the results from our in vitro experiments using retroviral-mediated cohesin knockdown, we decided to model cohesin loss of function in vivo. First, we analyzed cohesin expression in a subset of cell types of the mouse bone marrow. As expected, for a protein complex that is essential for mitosis, little variation was detected in hematopoietic stem cells (HSCs), immature progenitors, and myeloid progenitors (Fig. 3 A). Strikingly, large differences were observed in more mature cell populations within the bone marrow. Cohesin expression was markedly lower in myeloid cells ($Cd11b^+/Gr1^+$) and moderately significantly increased in basophilic erythroblasts ($CD71^+/Ter119^+$) when compared with B cells ($B220^+$; Fig. 3 B).

To achieve effective and reversible cohesin knockdown in vivo, we used a recently developed shRNA mouse approach (Premsrirut et al., 2011; Takiguchi et al., 2013; Bolden et al., 2014). In these animals, a single copy of an shRNA embedded in the 3′ untranslated region (UTR) of a GFP transgene is knocked in at the collagen (Col1a1) locus downstream of a tetracycline (Tet)-responsive element (TRE; Fig. 3 C). This shRNA animal model can subsequently be crossed to variants of Tet transcriptional activators (tTAs) or reverse tTAs (rtTAs). The resulting mouse model allows for inducible, reversible, and traceable expression of shRNAs in vivo. We generated shRNA mice for three members of the cohesin complex, Rad21, Smc1a, and Stag2. These cohesin shRNA mice were crossed to a $ROSA26^{(M2rtTA/+)}$ mouse to achieve ubiquitous and inducible systemic cohesin knockdown. To test this system, we provided doxycycline-enriched nutrition and checked for GFP expression in the bone marrow after 10 d. In all three cohesin shRNA mouse models GFP expression was robust (Fig. 3 D). No obvious differences were observed between control (Renilla) and cohesin shRNA in bone marrow, peripheral blood, spleen, and thymus (Fig. 3, D and E). As we used a systemic rtTA model, we also confirmed GFP (shRNA) expression (by immunohistochemical evaluation) in a variety of nonhematopoietic organs, including liver, skin, and intestine (not depicted). Next, we tested whether these high levels of GFP expression corresponded to efficient knockdown

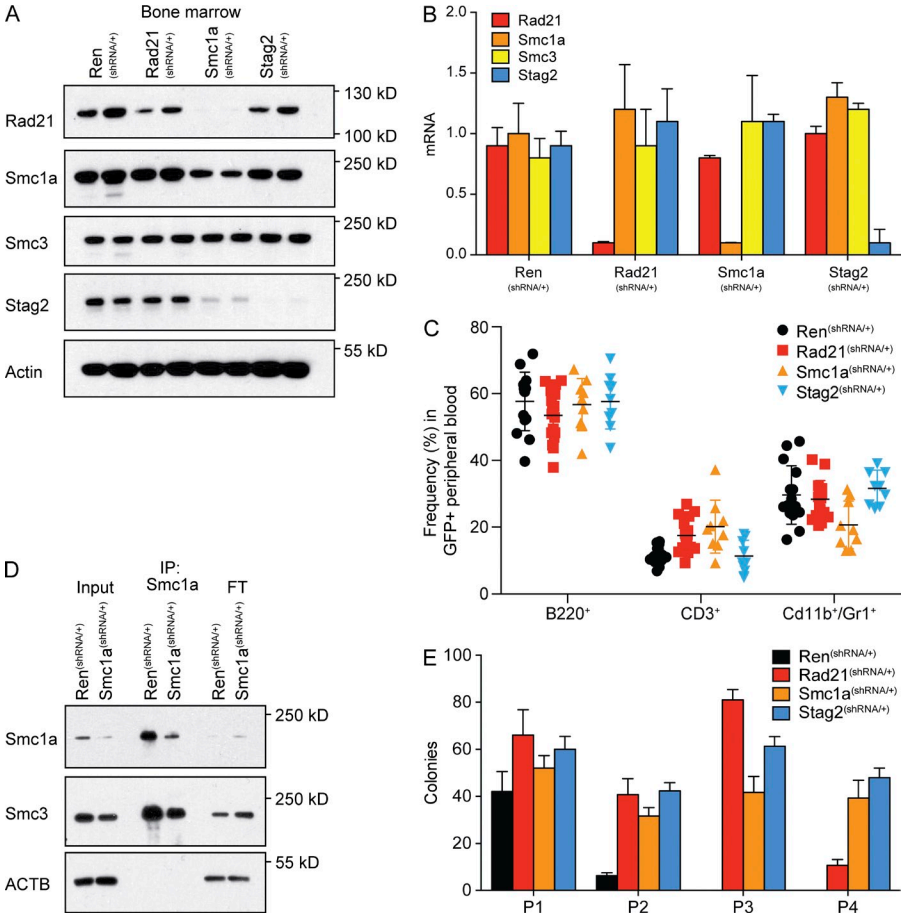


**Figure 4. Efficient in vivo silencing of cohesin does not lead to acute phenotypes.** (A) GFP+ cells were sorted from total bone marrow from Renilla$^{(shRNA/+)}$, Rad21$^{(shRNA/+)}$, Smc1a$^{(shRNA/+)}$, and Stag2$^{(shRNA/+)}$ mice ($n$ = 2). Protein was extracted and blotted for the indicated antibodies. (B) Erythroid progenitors (GFP+, CD71+/Ter119+) were FACS sorted from bone marrow of mice ($n$ = 3) that were exposed to doxycycline for 10 d. qRT-PCR was performed (using Actin B as reference), and cohesin knockdown was compared with Renilla control animals. (C) Animals ($n$ = 9) were exposed to doxycycline for 10 d and blood was drawn. FACS analysis is shown for B (B220+), T (CD3+), and myeloid cells (Cd11b+/Gr1+). (D) c-Kit+ cells from Renilla$^{(shRNA/+)}$ and Smc1a$^{(shRNA/+)}$ mice were cultured for 6 d. Smc1a protein was immunoprecipitated and blotted for indicated antibodies (IP, immunoprecipitation; FT, flow through). (E) Bone marrow of Renilla$^{(shRNA/+)}$, Rad21$^{(shRNA/+)}$, Smc1a$^{(shRNA/+)}$, and Stag2$^{(shRNA/+)}$ mice ($n$ = 3) was plated in methylcellulose containing doxycycline and replated for four passages. Error bars indicate SD.

in various cellular compartments. We tested knockdown of the mRNA in the thymus (T cells and progenitors) by Western blot analysis (Fig. 3 F).

In addition, we tested knockdown of the mRNA and protein in the bone marrow using Western blot and qRT-PCR (Fig. 4, A and B). Strikingly, in the Smc1a$^{(shRNA/+)}$ mice we not only observed a strong reduction of the intended mRNA (Smc1a), but also a significant decrease of the associated protein members of the cohesin complex, reminiscent of studies in different cellular systems (Vass et al., 2003; Laugsch et al., 2013). Despite this significant reduction of cohesin protein levels, FACS analysis of control and cohesin knockdown mice did not detect significant differences in peripheral blood cellular/mononuclear elements (Fig. 4 C). Likewise, no differences in complete blood counts of cohesin mice were observed at this stage (not depicted).

Furthermore, we did not detect gross chromosomal instability when we compared karyotype analysis of c-Kit+ progenitor cells of Renilla$^{(shRNA/+)}$, Rad21$^{(shRNA/+)}$, Smc1a$^{(shRNA/+)}$, and Stag2$^{(shRNA/+)}$ animals (not depicted). This can be explained by the fact that despite efficient knockdown of Rad21, Smc1a, or Stag2, the remaining proteins will continue to form a functional cohesin complex. We then evaluated this hypothesis with Smc1a and confirmed that the remaining Smc1a protein formed a complex with Smc3, allowing proper sister chromatid separation (Fig. 4 D). Finally, we sought to verify that the in vivo reduction of Rad21, Smc1a, and Stag2 is comparable with retroviral knockdown in our previous experiments. To test this, we plated bone marrow from Rad21$^{(shRNA/+)}$, Smc1a$^{(shRNA/+)}$, and Stag2$^{(shRNA/+)}$ mice in methylcellulose. Bone marrow from all three cohesin shRNA mice replated for four passages (compared with two for Renilla bone marrow; Fig. 4 E). These results indicate that significantly reduced expression of cohesin can be tolerated in vivo, providing us with the ability to further probe for cohesin functions in stem cell differentiation and transformation.

## Cohesin silencing leads to alterations in myeloid/erythroid differentiation

To monitor progressive changes in the hematopoietic system of cohesin knockdown mice, we generated a cohort of Tet-on rtTA shRNA animals that were continuously exposed to doxycycline starting at 6 wk of age. At several time points we performed whole body necropsy on these animals followed by a thorough analysis of the hematopoietic system. First, we confirmed that GFP (and therefore shRNA) expression is stable over time in the mouse models we generated. We analyzed frequency of GFP-expressing cells in the hematopoietic organs of mice that were exposed to doxycycline for 30 d. In all organs, GFP expression remained stable; interestingly, we

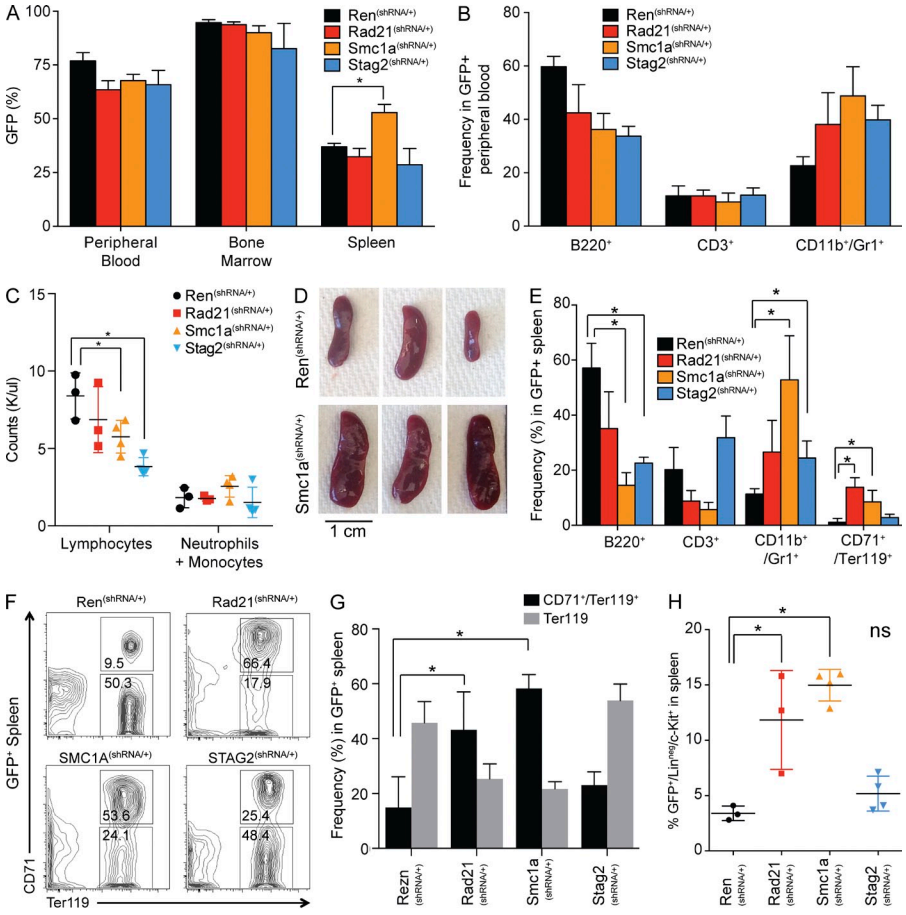


**Figure 5. Cohesin knockdown leads to changes in the myeloid/erythroid lineage in blood and spleen.** (A) Frequency of GFP+ cells as measured by flow cytometry (*, $P < 0.05$). (B) Flow cytometry analysis of peripheral blood from Renilla$^{(shRNA/+)}$, Rad21$^{(shRNA/+)}$, Smc1a$^{(shRNA/+)}$, and Stag2$^{(shRNA/+)}$ mice ($n = 3$) for the indicated antibodies. (C) Absolute numbers of lymphocytes and neutrophils/monocytes are plotted for the indicated genotypes (*, $P < 0.05$). (D) Representative spleens from Smc1a$^{(shRNA/+)}$ mice exposed to doxycycline for 30 d. (E) Flow cytometry analysis of spleen from Renilla$^{(shRNA/+)}$, Rad21$^{(shRNA/+)}$, Smc1a$^{(shRNA/+)}$, and Stag2$^{(shRNA/+)}$ mice ($n = 3$; *, $P < 0.05$) for the indicated antibodies. (F) Representative FACS analysis of the spleen of GFP+ basophilic erythroblasts (CD71+/Ter119+) and orthochromatophilic erythroblasts (Ter119+) for the indicated genotypes. (G) Quantification of GFP+ basophilic erythroblasts (CD71+/Ter119+) and orthochromatophilic erythroblasts (Ter119+) in spleens ($n = 3$) in animals of the indicated genotype that were exposed to doxycycline for 30 d (*, $P < 0.05$). (H) Frequencies of GFP+/Lineage−/c-Kit+ cells as measured in the spleens of the indicated genotypes ($n = 3$; *, $P < 0.05$). Error bars indicate SD.

observed an increase in frequency of GFP-expressing cells in the spleen of Smc1a$^{(shRNA/+)}$ animals (Fig. 5 A). This prompted us to further investigate the lineages present in the spleen, bone marrow, and blood of Rad21$^{(shRNA/+)}$, Smc1a$^{(shRNA/+)}$, Stag2$^{(shRNA/+)}$, and Renilla$^{(shRNA/+)}$ control mice. Indeed, lineage skewing was apparent by FACS analysis (Fig. 5 B) and peripheral blood mononuclear cell differential counts (Fig. 5 C) in Rad21$^{(shRNA/+)}$, Smc1a$^{(shRNA/+)}$, and Stag2$^{(shRNA/+)}$ animals compared with Renilla$^{(shRNA/+)}$ mice. Morphologically, several animals displayed splenomegaly, which was most apparent in Smc1a$^{(shRNA/+)}$ mice (Fig. 5 D). FACS analysis of the spleens of Rad21$^{(shRNA/+)}$, Smc1a$^{(shRNA/+)}$, and Stag2$^{(shRNA/+)}$ animals showed a decrease in the proportion of B cell population (B220+), coupled to an increase in myelomonocytic (Cd11b+/Gr1+) and erythroid cells (CD71+/Ter119+; Fig. 5 E).

A marked erythroid expansion with increased amounts of early erythroid elements (CD71+/Ter119+) was observed in the spleen of Rad21$^{(shRNA/+)}$ and Smc1a$^{(shRNA/+)}$ animals (Fig. 5, F and G). These results suggested the presence of erythroid colonies in spleen samples of these animals. In addition, we found a significant increase of Lineage−/c-Kit+ cells in spleens of Rad21$^{(shRNA/+)}$ and Smc1a$^{(shRNA/+)}$ mice (Fig. 5 H). The combined findings, namely the increase of both erythroid and c-Kit+ cells, indicate myeloid metaplasia, also known as extramedullary hematopoiesis, in the splenic parenchyma, a phenomenon observed in several preleukemic mouse models (Moran-Crusio et al., 2011; Celik et al., 2015).

Next, we investigated the bone marrow, where we observed a decrease in the Ter119+ cell population in the GFP+ bone marrow of Rad21$^{(shRNA/+)}$ and Smc1a$^{(shRNA/+)}$ animals (Fig. 6 A). The increase in myeloid element in the spleen and bone marrow prompted us to investigate the progenitor compartment in the bone marrow of affected animals. Here, we noticed an expansion in the frequency of granulocyte-macrophage progenitors (GMPs; Lineage−/c-Kit+/Sca-1−/Cd34+/FcRII/III+) in the GFP+ population of Rad21$^{(shRNA/+)}$ and Smc1a$^{(shRNA/+)}$ mice (Fig. 6, B and C). This was accompanied by a decrease in megakaryocyte-erythrocyte progenitors (Lineage−/c-Kit+/Sca-1−/Cd34−/FcRII/III−; Fig. 6, B and C).

An additional phenotype we observed was an increase in nuclear size in sorted Lineage−/c-Kit+ progenitor cells (Fig. 6, D and E). The exact cause and/or consequence of this phenomenon is unknown, but it has been previously associated with cohesin loss of function in other cell types (Hoque and Ishikawa, 2002; Sofueva et al., 2013). The apparent increase in nuclear size was also seen in other elements of the hematopoietic system of cohesin knockdown mice (not depicted). Of note, the increase in nuclear volume was not associated with increase of genomic material or instability, as confirmed by conventional cytogenetic analysis on metaphase spreads,

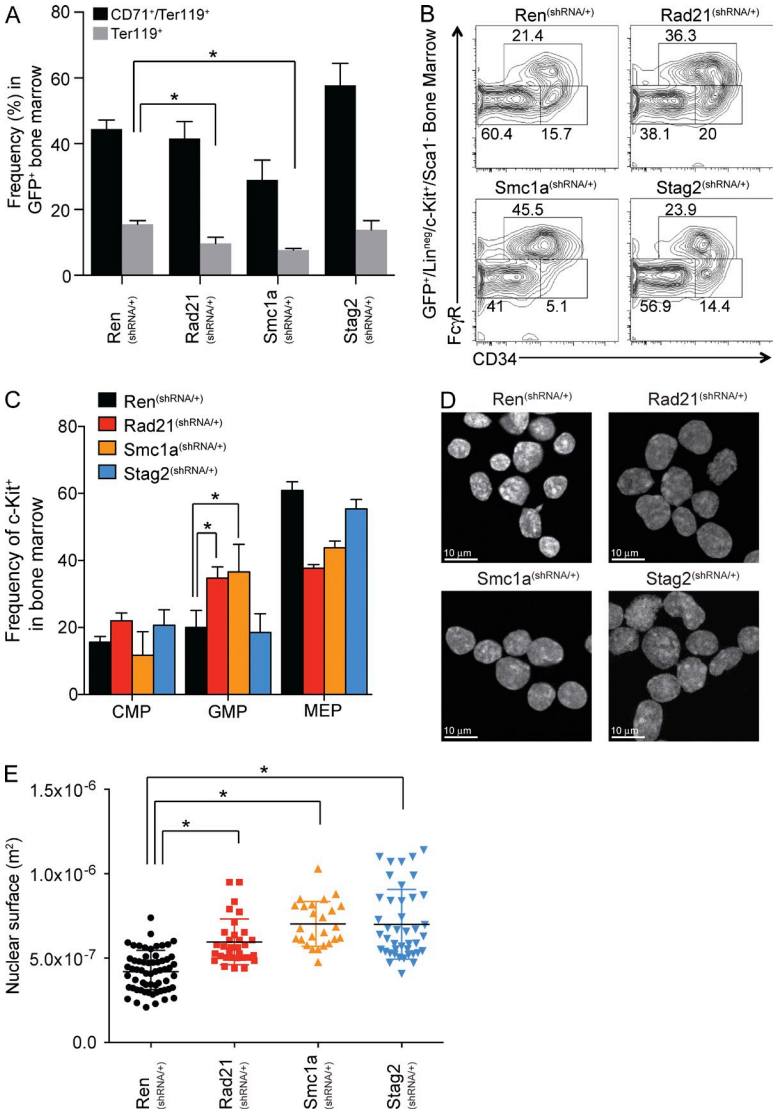


**Figure 6. Cohesin knockdown induces myeloid progenitor skewing and increases the size of the nucleus.** (A) Quantification of flow cytometry of bone marrow of animals ($n = 3$) of the indicated genotype (*, $P < 0.05$). (B) FACS analysis of bone marrow of cohesin knockdown mice (doxycycline 30 d, $n = 3$) for myeloid progenitors (GFP$^+$/Lin$^-$/c-Kit$^+$/Sca1$^-$). (C) Quantification of myeloid progenitors in the bone marrow of mice ($n = 3$) with the indicated genotype (*, $P < 0.05$). (D) GFP$^+$/c-Kit$^+$ cells were sorted from mouse ($n = 3$) bone marrow of control and cohesin knockdown (10 d of doxycycline). Cells were fixed on glass slides and stained with DAPI. (E) Quantification of nuclear size of GFP$^+$/c-Kit$^+$ cells for the indicated genotypes. Surface area of nuclei was measured using DAPI intensity with ImageJ (National Institutes of Health; *, $P < 0.05$). Error bars indicate SD.

verifying a normal diploid karyotype (not depicted). Collectively, these results demonstrate that knockdown of cohesin subunits can alter hematopoiesis with an apparent bias toward the myeloid hyperplasia, suggesting a role for cohesin in myeloid differentiation.

### Cohesin knockdown induces differentiation skewing of HSCs

The changes found in the differentiated and progenitors cells prompted us to address the impact of cohesin knockdown on HSCs. We decided to focus on two out of the three mouse models we created, Smc1a$^{(shRNA/+)}$ and Stag2$^{(shRNA/+)}$. We chose Smc1a and Stag2 to include one core ring component, Smc1a, and one associated protein, Stag2. Indeed, even after a short period of cohesin gene knockdown (10 d), we observed distinct changes in the HSC compartment of Smc1a$^{(shRNA/+)}$ and Stag2$^{(shRNA/+)}$ mice (Fig. 7 A). First, we noted that cohesin knockdown did not significantly impact the Lineage$^-$ Sca1$^+$ c-Kit$^+$ (LSK) cells, a population which is composed of HSCs and multipotent progenitors (MPPs; not depicted). Next, we analyzed the effect of cohesin knockdown in long-term HSCs (LT-HSCs) and MPPs. A striking reduction of shRNA-expressing phenotypic long-term (CD150$^+$) and short-term (CD150$^-$/CD48$^-$) HSC subsets was observed, evaluated by expression, frequency (Fig. 7 B), and absolute counts (Fig. 7 C). In the Smc1a$^{(shRNA/+)}$ mouse model, this loss of HSCs was compensated by a gain in MPPs and specifically the CD150$^+$/CD48$^+$ MPP subset (Fig. 7 C). A similar phenotype has been described previously in an Flt3-ITD animal model (Chu et al., 2012).

Next we wanted to identify the transcriptional changes, which underlie the phenotypic changes that we observed in the Lineage$^-$ Sca1$^+$ c-Kit$^+$ compartment (LSK subset, comprised of HSCs and MPP cells) of Smc1a and Stag2 knockdown mice. We performed gene expression analysis (using RNA sequencing) of purified LSK cells (GFP$^+$/Lineage$^-$/Sca1$^+$/c-Kit$^+$) from Renilla$^{(shRNA/+)}$, Smc1a$^{(shRNA/+)}$, and Stag2$^{(shRNA/+)}$ mice. We again confirmed that the shRNA-expressing cells (as measured by expression of GFP) indeed

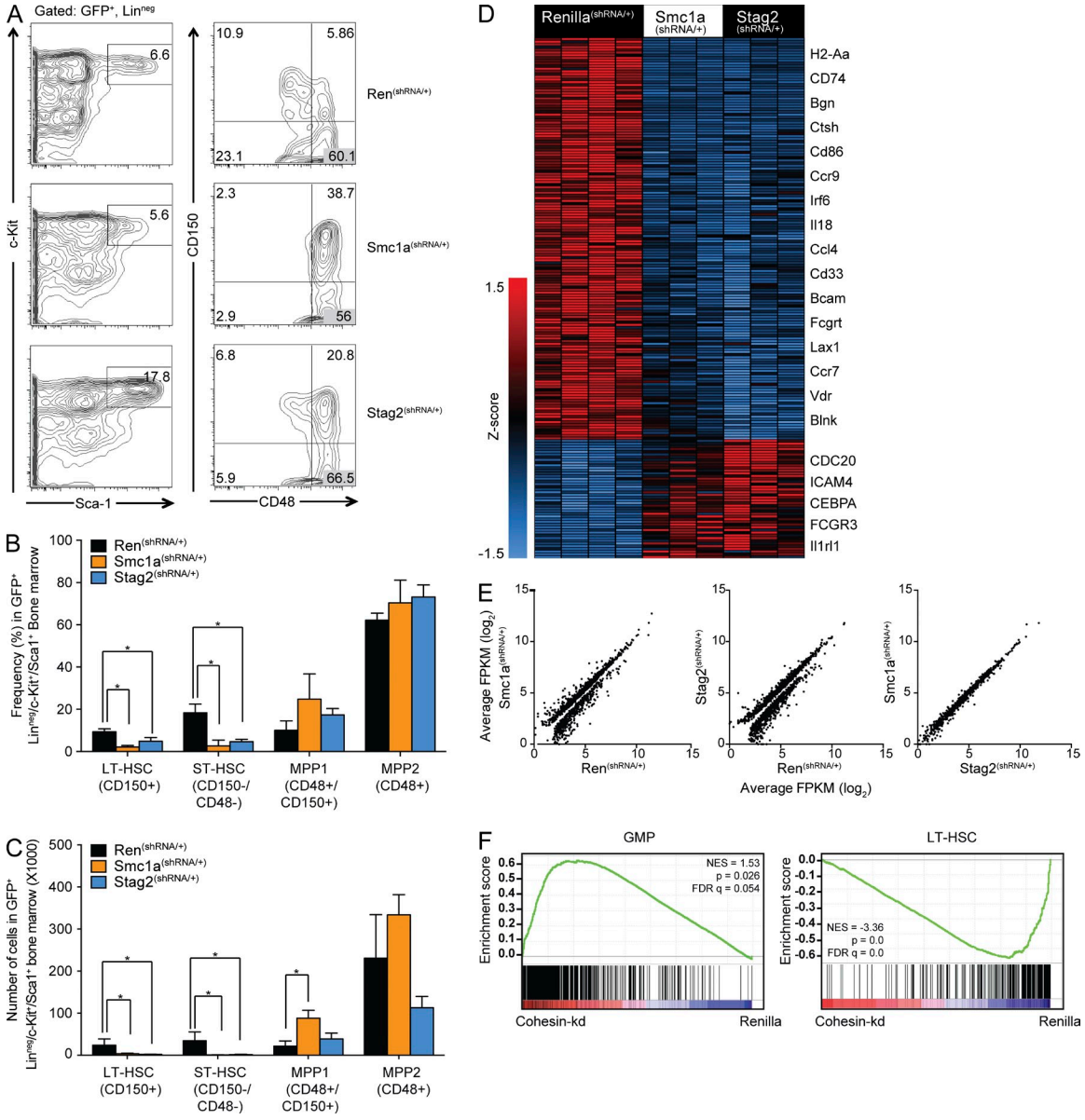


**Figure 7. Rapid skewing of HSCs induced by cohesin knockdown.** (A) Mouse bone marrow ($n = 3$; genotype is indicated) was isolated and stained with antibodies for lineage markers, c-Kit, Sca1, CD48, and CD150. The stem cell compartment was visualized by gating as follows: GFP$^+$ > Lineage$^-$ > c-Kit$^+$/Sca1$^+$ (LSK). Left panels indicate the frequency of LSK cells in the indicated genotype. Right panels show stem cell and MPP compartment, CD150$^+$ LT-HSCs, CD150$^-$/CD48$^-$ short-term HSCs, CD150$^+$/CD48$^+$ MPP1, and CD48$^+$ MPP2. (B) Quantification of changes in stem cell compartment of Smc1a$^{(shRNA/+)}$ and Stag2$^{(shRNA/+)}$ mice ($n = 3$; *, $P < 0.05$). (C) Quantification of absolute cell number of HSCs and MPPs in the bone marrow of cohesin knockdown mice ($n = 3$; *, $P < 0.05$). (D) Gene expression analysis by RNA sequencing of sorted LSK cells of cohesin knockdown bone marrow. GFP$^+$/Lin$^-$/Sca1$^+$/c-Kit$^+$ cells were sorted from bone marrow of mice ($n = 3$ or 4) exposed to doxycycline for 10 d. Heat map shows genes that are significantly ($P < 0.05$) differentially expressed with a cutoff of 1.5 FC. (E) Scatter plots of FPKM obtained from RNA-seq results from Renilla$^{(shRNA/+)}$, Smc1a$^{(shRNA/+)}$, and Stag2$^{(shRNA/+)}$ LSK cells. (F) GSEA of RNA-seq data comparing Renilla with cohesin knockdown. Cohesin knockdown LSK cells are enriched for a GMP signature and depleted for an LT-HSC signature. Error bars indicate SD.

have a very potent knockdown of the intended target genes, Smc1a and Stag2 (not depicted). Next, we focused on the significantly differentially expressed genes (FPKM > 5, fold change [FC] > 1.5, and $P < 0.05$) in the various genotypes (Table S3). In the Smc1a$^{(shRNA/+)}$ LSK cells, we found up-regulation and down-regulation of 257 and 338 genes, respectively, compared with the Renilla control. In the Stag2$^{(shRNA/+)}$ LSK cells, we found up- and down-regulation of 390 and 480 genes, respectively, compared with Renilla control. By comparing the gene expression profiles of Smc1a$^{(shRNA/+)}$ with Stag2$^{(shRNA/+)}$, few differentially expressed genes were found (53 down and 125 up). Indeed, Smc1a and Stag2 appear to regulate an

identical expression program in LSK cells (Fig. 7, D and E). Interestingly, genes found up-regulated in cohesin knockdown LSK cells are associated with a myeloid differentiation program, including the *Fcgr3* and *Cebpa* genes, encoding key regulators of myelopoiesis (Fig. 7 D). At the same time, we observed down-regulation of genes involved in lymphoid development (including *Blnk*, *Lax1*, and *Cd86*). These data suggested that cohesin gene knockdown LSK cells are primed to differentiate toward the myeloid lineage, in agreement with our in vivo phenotype of the studied animals. This was further confirmed by an unbiased analysis of the gene expression changes by gene set enrichment analysis (GSEA). Such analysis showed that LSK cells from Smc1a$^{(shRNA/+)}$ and Stag2$^{(shRNA/+)}$ mice showed an aberrant and premature commitment to the myeloid lineage based on their gene expression signature (Fig. 7 F). In agreement with the loss of phenotypic HSCs in these animals, LSK cells have lost expression of genes that normally comprise a signature of LT-HSCs. These data show that cohesin knockdown in LSK cells leads to transcriptional changes that are associated with a differentiation bias during early stages of hematopoiesis.

### Cohesin silencing leads to aberrant chromatin accessibility

Cohesin is known to be involved in several processes that regulate transcription and gene expression. Cohesin binds to CTCF and is found together with CTCF on chromatin (Parelho et al., 2008; Wendt et al., 2008). More recently, it was shown that cohesin clusters are found at sites with high chromatin accessibility measured by DNase I hypersensitivity (Yan et al., 2013) assays. Therefore we decided to apply ATAC sequencing, a genome-wide mapping of chromatin accessibility. We performed ATAC sequencing on purified stem/progenitor LSK cells from Renilla$^{(shRNA/+)}$ and Stag2$^{(shRNA/+)}$ mice to map changes in chromatin accessibility (Buenrostro et al., 2015). ATAC-seq analysis showed a large number of changes between Renilla$^{(shRNA/+)}$ and Stag2$^{(shRNA/+)}$ samples (Fig. 8, A and B; and Table S4). Changes in chromatin accessibility were pronounced in genes that were up-regulated in cohesin knockdown LSK cells, like Fc-γ receptor (*Fcgr3* and *Fcgr4*) and Myeloperoxidase (*Mpo*; Fig. 8, C and D). These genes are highly expressed in myeloid cells, suggesting that the cohesin complex plays a role in the regulation of myeloid differentiation through chromatin accessibility. In addition, we found that genes that were expressed in lower levels in cohesin knockdown cells (like *Cd74*) lose DNA accessibility (Fig. 8, C and D). Next, we compared RNA expression and chromatin accessibility in an unbiased way. We found that increased chromatin accessibility around promoter regions indeed correlates with significant increased expression, and the reverse is also true (Fig. 8 E). Furthermore, we performed GSEA with the ATAC-seq peaks enriched in either Renilla$^{(shRNA/+)}$ or Stag2$^{(shRNA/+)}$ LSK cells. Here we observed that peaks enriched in Stag2$^{(shRNA/+)}$ LSK cells correlate with the GMP signature that we found before to be enriched in the RNA sequencing data (Fig. 8 F). Furthermore, we used an unbiased approach to test whether the changes in chromatin accessibility reflected a change in the cellular state (McLean et al., 2010). Regions that were more accessible in the Stag2 knockdown cells correlated with GO terms for myeloid differentiation and erythroid development, in line with our findings in vivo (Fig. 8 G and Table S5). This is specific for cohesin knockdown cells, as we don't find the same enrichment in the regions that are more accessible in Renilla control LSK cells (Table S5). GSEA and GO term analysis confirmed the notion that cohesin knockdown LSK cells are committed to differentiate along the myeloid lineage. Finally, we analyzed the genomic sequence in the more accessible regions of the cohesin cells for enrichment of transcription factor motifs (Imrichová et al., 2015). We found that the most enriched transcription factor motif is the GATA factor motif (Fig. 8 H). GATA1 is a master regulator of primitive and definitive hematopoiesis, and erythropoiesis and is often mutated in cancer (Crispino, 2005). In our ATAC-seq data, we also found increased accessibility in the GATA1 locus in Stag2 knockdown LSK cells (Fig. 8 C). Collectively, these data suggest that cohesin knockdown leads to changes in chromatin accessibility in genes that are expressed in the myeloid lineage, possibly through involvement of GATA transcription factors.

### Silencing of cohesin complex genes leads to an MPN/myeloid disorder

The ageing cohort of cohesin gene knockdown was monitored by FACS analysis of peripheral blood at regular intervals. During these routine examinations, we found that several animals showed a marked expansion of myeloid elements (granulocytic > monocytic) in the peripheral blood, consistent with myeloid hyperplasia (Cd11b$^{+}$/Gr1$^{+}$; Fig. 9, A and B [I–III]). Necropsy was performed on a subset of the animals to allow for a more in-depth analysis. A first gross morphological indication for an underlying hematopoietic disorder was the presence of varying degrees of splenomegaly. Fig. 9 depicts an example of the phenotype (organomegaly) of an Smc1a$^{(shRNA/+)}$ animal in comparison to an age-matched Renilla$^{(shRNA/+)}$ control (Fig. 9 C). Histological evaluation confirmed that the splenic architecture was compromised by marked to moderate red pulp expansion, exhibiting myeloid metaplasia (extramedullary hematopoiesis; Fig. 9 B, IV). The hematopoietic elements were composed of numerous myelomonocytic cells, including frequent immature forms, alternating with variable amounts of erythroid precursors, forming occasional erythroid islands and frequent megakaryocytes (Fig. 9 B, V and VI). Gross evaluation of bone specimens of the affected Smc1a$^{(shRNA/+)}$ animals demonstrated "pale appearing" bones and histological evaluation showed a hypercellular bone marrow with erythroid and megakaryocytic hypoplasia and marked myeloid hyperplasia (Fig. 9, B [VII] and D). The myeloid elements were predominantly medium to large in size, with open chromatin, crisp and irregular nuclear membrane, and variable amounts of amphophilic cytoplasm, focally imparting myelomonocytoid features (Fig. 9 B, VIII and IX). Peripheral blood differential count analysis confirmed a significant increase in neutrophil numbers (Fig. 9 E)

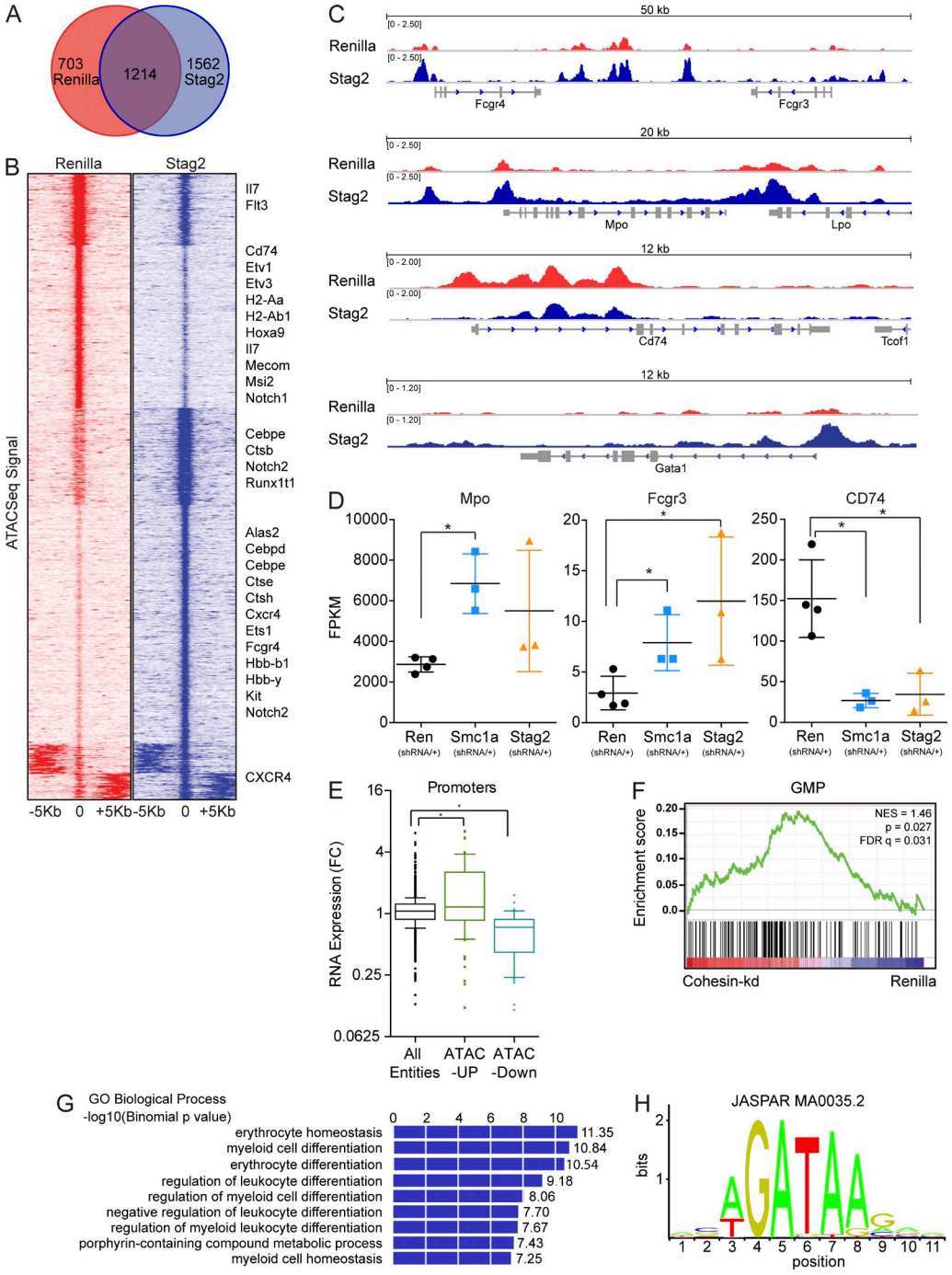


**Figure 8. Cohesin silencing leads to changes in chromatin accessibility in LSK cells.** (A) Venn diagrams of ATAC-seq peaks (peak score > 25) found in LSK cells isolated from Renilla$^{(shRNA/+)}$ and Stag2$^{(shRNA/+)}$ mice. (B) Heat map of peaks found significantly enriched (FC(abs) > 2, P < 0.05) Renilla$^{(shRNA/+)}$ and Stag2$^{(shRNA/+)}$ ATAC-seq centered on the peak maximum. (C) Changes in chromatin accessibility in key myeloid differentiation genes (*Mpo*, *Fcgr3/4*, and *GATA1*). Tracks showing increase in ATAC-seq signal on *MPO* and *FCGR3/4* genes in LSK cells from Renilla$^{(shRNA/+)}$ and Stag2$^{(shRNA/+)}$ mice. Loss of ATAC-seq signal in the stem cell gene *CD74* in LSK cells from Renilla$^{(shRNA/+)}$ and Stag2$^{(shRNA/+)}$ mice. (D) Changes in gene expression in LSK cells from cohesin knockdown mice. Indicated are FPKM values for MPO, FCGR3, and CD74 as obtained from RNA sequencing in LSK cells for the indicated genotypes (*, P < 0.05). (E) RNA expression correlates with chromatin accessibility. Changes in RNA expression (RNA sequencing) of genes that have either increased (Up) or decreased (Down) chromatin accessibility (ATAC-sequencing) at their promoter are plotted (*, P < 0.05). (F) GSEA of Stag2 knockdown enriched ATAC-seq peaks. (G) GO term enrichment of biological processes with peaks (FC(abs) > 2, P < 0.05) that are unique in the Stag2$^{(shRNA/+)}$ ATAC-seq. (H) Result from transcription factor motif enrichment in peaks (FC(abs) > 2, P < 0.05) unique in the Stag2$^{(shRNA/+)}$ ATAC-seq. Error bars indicate SD.

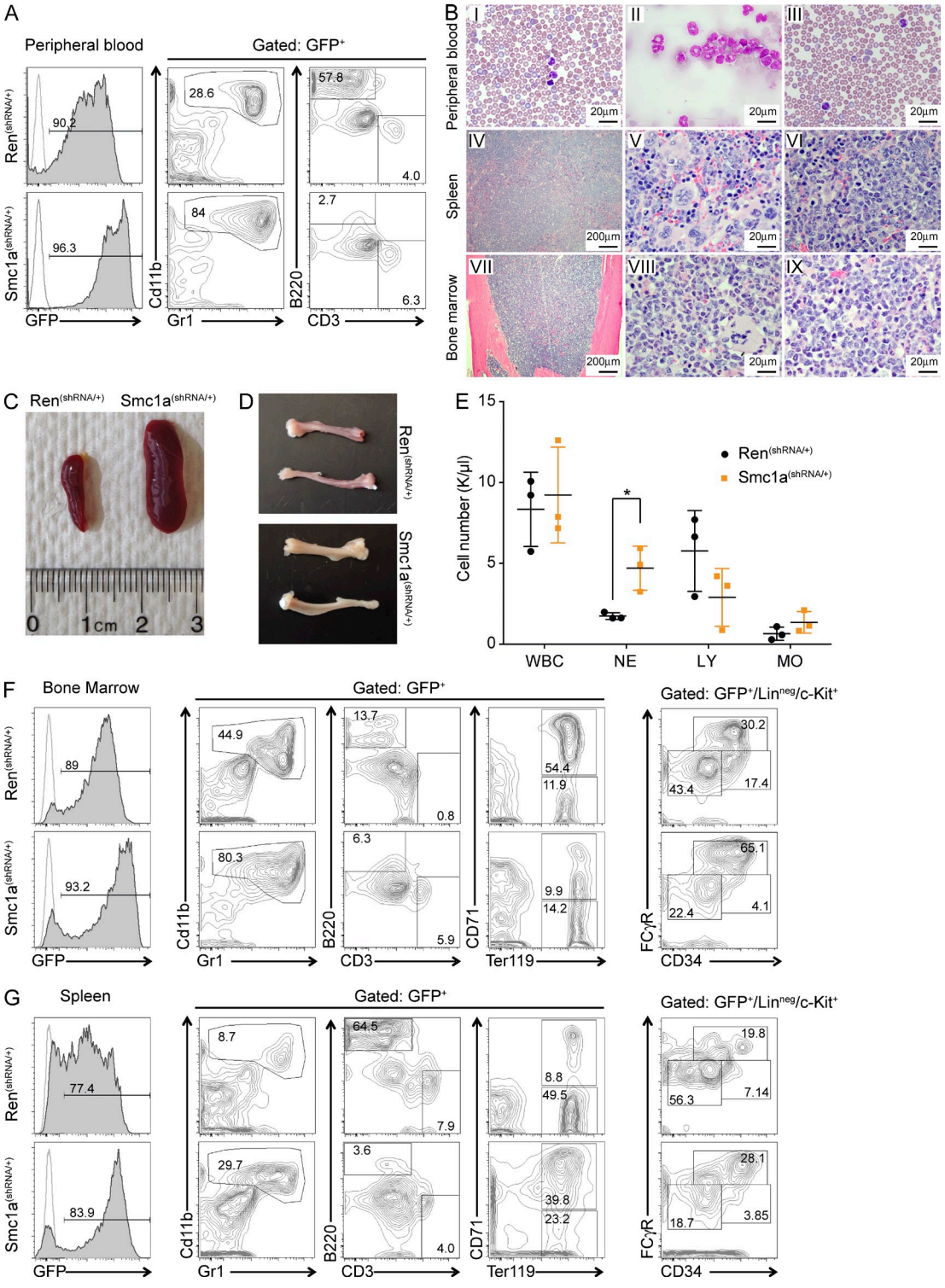


**Figure 9. MPNs in aged Smc1a$^{(shRNA/+)}$ mice.** (A) FACS analysis of peripheral blood of age-matched Renilla$^{(shRNA/+)}$ control and Smc1a$^{(shRNA/+)}$ mouse (antibodies are indicated). (B) Histological analysis of peripheral blood, spleen, and bone marrow from Smc1a$^{(shRNA/+)}$ mouse. Peripheral blood was stained with Wright-Giemsa. Spleen and bone marrow were stained with H&E. (C) Representative spleen of aged Smc1a$^{(shRNA/+)}$ mouse. (D) Representative femur and tibia of aged Smc1a$^{(shRNA/+)}$ mouse. (E) Blood count of diseased Smc1a$^{(shRNA/+)}$ mice. WBC, white blood cells; NE, neutrophils; LY, lymphocytes; and MO, monocytes (*, $P < 0.05$). (F and G) FACS analysis of bone marrow and spleen of representative aged Smc1a$^{(shRNA/+)}$ mice. (left) GFP expression. (middle) Antibody staining for myeloid (Cd11b$^+$/Gr1$^+$), B (B220$^+$), T (CD3$^+$), and erythroid cells (CD71$^+$/Ter119$^+$ and Ter119$^+$) is indicated. (right) FACS staining for myeloid progenitors (GFP$^+$/Lin$^-$/c-Kit$^+$/Sca1$^-$) is plotted. Error bars indicate SD.

in the affected animals, further supporting that Smc1a silencing promotes a clinical picture consistent with an MPN. Flow cytometry analysis performed on peripheral blood spleen and marrow specimens revealed similar but more pronounced phenotypes in these animals compared with the younger animal cohort. All three compartments demonstrated a marked increase in myeloid cells ($Cd11b^+/Gr1^+$), which was accompanied by a decrease in lymphoid elements, particularly $B220^+$ B cells, (Fig. 9, A, F, and G). Composition of medullary and extramedullary hematopoiesis differed from case to case, with a subset of spleen specimens showing trilineage maturing hematopoiesis with erythroid predominance and intact erythroid islands, immunophenotypically confirmed by increased $CD71^+/Ter119^+$ cells, whereas bone marrow hematopoietic elements demonstrated erythroid hypoplasia confirmed by a decrease in $CD71^+/Ter119^+$ cells (Fig. 9, F and G). Notably, a striking increase of GMPs ($GFP^+/Lineage^-/c\text{-}Kit^+/Sca\text{-}1^-/Cd34^+/FcRII/III^+$) was found in these bone marrow specimens (Fig. 9 F, right), in agreement with previous experiments (Fig. 6 C). In spleen specimens of $Smc1a^{(shRNA/+)}$ mice, the immature myelomonocytic proliferation was immunophenotypically confirmed by an increase in $GFP^+/Lineage^-/c\text{-}Kit^+/Sca\text{-}1^-$ cells (Fig. 9 G, right).

Encouraged by these results, we decided to generate mice with a more potent disruption of the cohesin complex. Our rationale for this is the fact that *SMC1A* and *STAG2* mutations found in patients potentially generate strong loss of function alleles because these genes are located on the X chromosome. In addition, simultaneous down-regulation of the mRNA level of multiple cohesin members has been observed in AML samples (Thota et al., 2014). To obtain compound shRNA mice that target two cohesin subunits simultaneously, we intercrossed $Smc1a^{(shRNA/+)}$ and $Stag2^{(shRNA/+)}$ mice. Compound $Smc1a^{(shRNA)}/Stag2^{(shRNA)}$ did not show any deleterious phenotypes, although an effective knockdown was confirmed (Fig. 10 A). Short-term exposure to doxycycline (22 d) caused splenomegaly (not depicted) and lineage skewing (Fig. 10 B). Over time, $Smc1a^{(shRNA)}/Stag2^{(shRNA)}$ animals showed again significant lineage skewing in the peripheral blood, namely myeloid hyperplasia ($Cd11b^+/Gr1^+$) and lymphopenia (decrease in $B220^+$ cells; Fig. 10 C). FACS analysis of these animals revealed a very similar yet more pronounced phenotype compared with the $Smc1a^{(shRNA/+)}$ mouse (not depicted). Spleens of aged compound $Smc1a^{(shRNA)}/Stag2^{(shRNA)}$ animals were enlarged compared with control animals and showed disrupted morphology (Fig. 10, D and E). Diseased animals demonstrated signs of anemia, as exemplified by peripheral blood counts (Fig. 10 F).

In summary, these experiments effectively demonstrate that silencing of the cohesin complex alters stem cell homeostasis, predominantly affecting the myeloid component, leading to disturbances in myeloid proliferation and differentiation closely resembling the clinical picture of a myeloid disorder/myeloid neoplasm. In addition, our study describes the first in vivo models that demonstrate a tumor-suppressive role for the cohesin complex.

## DISCUSSION

AML is a genetically diverse disease. Fusion genes and mutations in many lineage-specific transcription factors and epigenetic regulators have been uncovered. Recently, mutations in the cohesin (Rad21, Smc1a, Smc3, and Stag2) complex have been identified in de novo and secondary AML samples, as well as many solid tumors (Leiserson et al., 2015). Many of these mutations are predicted (and shown here) to result in loss of function of the affected protein. This is very surprising, as all cohesin genes are essential in every organism tested from yeast to mice. Indeed, $Rad21^{-/-}$ animals are not viable (Xu et al., 2010); however, conditional knockout of Rad21 in postmitotic thymocytes does not affect survival (Seitan et al., 2011). These findings support the notion that cohesin proteins are present at high levels both in actively cycling and quiescent tissues (Wendt et al., 2008). In tumors, mutations in Smc3 and Rad21 are usually heterozygous, leaving one copy of the gene unaffected. Stag2 and Smc1a reside on chromosome X and are therefore not compensated by a wild-type protein when mutated in male patients. Similar in females, all mutations found in Stag2 were reported to be on the active (transcribed) X chromosome (Solomon et al., 2011). Surprisingly, even in an essential gene like Smc1a, a portion (~10%) of the alterations were found to be nonsense and/or frame-shift mutations, predicting a complete loss of protein function (http://www.cbioportal.org). How cells deficient for a cohesin subunit manage to correctly separate their chromosomes remains to be understood.

To model the loss of cohesin as seen in human malignancies, we generated three independent loss of function cohesin animals. As standard mouse knockout techniques create complete null alleles, we opted to generate three mouse models with inducible shRNA targeting cohesin complex members in vivo (Premsrirut et al., 2011). In these animals, we managed to efficiently suppress cohesin transcripts and reduce cohesin protein expression and function similar to that seen in human malignancies. Surprisingly, even in mice where we induced systemic cohesin knockdown, we did not observe detrimental effects, although we never reached a complete loss of expression in this model. We were surprised by the initial lack of survival phenotypes in cells with a very efficient reduction of the cohesin complex members. One explanation is the fact that during metaphase only a very small fraction of cohesin is required for SCC (Waizenegger et al., 2000). Apparently, the small amount of cohesin protein that remains in our shRNA mouse is most likely sufficient for proper SCC and successful mitosis. This is consistent with the fact that we did not observe overwhelming defects in SCC in cohesin knockdown cells. Another process cohesin is known to play a role in is DNA damage repair (Watrin and Peters, 2006). At this moment, no consensus exists on whether mutations in cohesin in human malignancies lead to genomic instability (Solomon et al., 2011; Balbás-Martínez et al., 2013; Li et al., 2015), although using our cohesin knockdown cells we did not observe changes of the overall karyotype. Similarly, human AML samples carrying cohesin mutations do

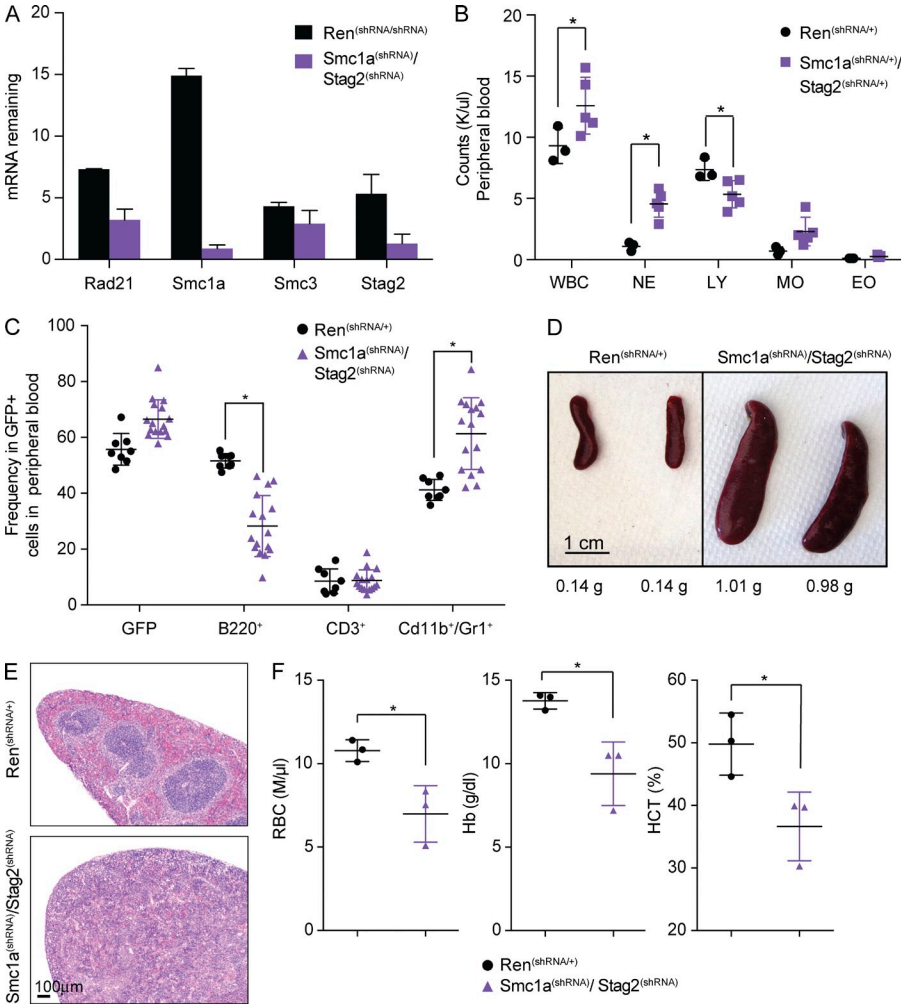


**Figure 10. MPNs and splenomegaly in Smc1a-Stag2 shRNA compound animals.** (A) qRT-PCR of sorted erythroblasts (GFP+/CD71+/Ter119+) from the bone marrow of Smc1a$^{(shRNA)}$/Stag2$^{(shRNA)}$ mice ($n = 3$) exposed to doxycycline for 22 d. (B) Changes in absolute numbers of white blood cells of Smc1a$^{(shRNA)}$/Stag2$^{(shRNA)}$ mice ($n = 5$) exposed to doxycycline for 22 d. Blood was analyzed by Hemavet. WBC, white blood cells; NE, neutrophils; LY, lymphocytes; MO, monocytes; and EO, eosinophils (*, $P < 0.05$). (C) Quantification of FACS analysis of Renilla$^{(shRNA/+)}$ ($n = 8$) and Smc1a$^{(shRNA)}$/Stag2$^{(shRNA)}$ ($n = 16$) mice for the indicated antibodies (*, $P < 0.05$). (D) Representative spleens of Smc1a$^{(shRNA)}$/Stag2$^{(shRNA)}$ animals after doxycycline exposure for 2–3 mo. Spleen weight is indicated below the organs. (E) H&E stain of a representative section of spleen of Renilla$^{(shRNA/+)}$ and Smc1a$^{(shRNA)}$/Stag2$^{(shRNA)}$ animals treated with docycycline for 2 mo. (F) Blood counts of Smc1a$^{(shRNA)}$/Stag2$^{(shRNA)}$ mice ($n = 3$) on doxycycline for 2–3 mo (*, $P < 0.05$). Error bars indicate SD.

not have an overt genomic instability phenotype (Cancer Genome Atlas Research Network, 2013).

As no differences are observed in steady state SCC and DNA damage response, we hypothesize that loss of cohesin complex member expression in human disease mainly affects higher-order chromatin structure and gene expression. The genome of eukaryotes is organized into structural domains that help establish regulatory interactions (Lieberman-Aiden et al., 2009; Dixon et al., 2012). The cohesin complex is one of the main factors involved in the stability of the three-dimensional organization of the chromatin. When cohesin is removed from cells, a general unfolding and disorganization of the chromatin is observed with associated changes in gene expression (Seitan et al., 2013; Sofueva et al., 2013; Mizuguchi et al., 2014). Changes in higher-order chromatin structure have been observed in disease, including cancer (Rickman et al., 2012). It is therefore not unconceivable that loss of cohesin in cancer leads to disruption of chromatin organization. Cohesin serves as a docking station for transcription factors, and its absence could therefore cause transcription factors to aberrantly activate genes (Yan et al., 2013). We postulate that cohesin mutations in AML mainly impact genome organization, adding a new layer of complexity to an already complicated disease. The chromatin accessibility data and correlation with gene expression changes presented here support this hypothesis.

AML is a disease that often originates in stem cells' hematopoietic system (Shlush et al., 2014). During the progression of the disease, clonal evolution is a common occurrence (Ding et al., 2012). Recently, several studies have identified mutations in the originating stem cell in AML (Genovese et al., 2014). Cohesin genes are among the genes that are mutated in the stem cells that are found in the bone marrow of AML patients (Ding et al., 2012; Jan et al., 2012). Here, we provide evidence that loss of cohesin indeed leads to increased self-renewal of stem cells in vitro. Cohesin knockdown mice display a skewing in their stem cell compartment in the bone marrow and show signs of extramedullary hematopoiesis in the spleen. All these phenotypes have been reported before in mouse models for AML (Lee et al., 2007; Moran-Crusio et al., 2011).

This is the first example of cohesin loss of function in a mammalian system. Strikingly, efficient (but not complete) silencing of cohesin is not detrimental to cellular homeostasis but leads to myeloproliferative disease, suggesting that there

are defined thresholds of cohesin expression and activity. This notion is consistent with the findings illustrated in the accompanying paper in this issue by Viny et al., where complete deletion of another cohesin member, Smc3, leads to lethal bone marrow aplasia, whereas Smc3 haploinsufficiency leads to enhanced self-renewal and AML in the background of Flt3-ITD. Our study is the first evidence that mutation of cohesin is a driving event in the initiation and progression of cancer and not merely a bystander. Furthermore, this suggests that cohesin loss could be therapeutically exploited. Cells carrying mutations in the cohesin complex are potentially more vulnerable to certain stressors or insults. The identification of cohesin synthetic lethal interactions could aid the development of new drugs, specifically targeting cohesin mutant cells. For this to be successfully introduced into the clinic, it is a prerequisite that AML patients are preselected based on their cohesin mutation status. Such a new class of drugs is very welcome in a disease such as AML, where very few targeted therapies are available at this moment.

## MATERIALS AND METHODS

**Western blot.** Protein was extracted from equal cell numbers in a high urea buffer (48% urea, 15 mM Tris-HCl, pH 7.5, 8.7% glycerin, 1% SDS, 0.004% bromophenol blue, and 143 mM β-mercaptoethanol). Protein levels were measured using the Bradford assay. Equal amounts of protein were loaded on NuPAGE Novex 4–12% Bis-Tris protein gel (NP0321; Life Technologies) and run with NuPAGE MOPS buffer (NP0001; Life Technologies). Proteins were transferred to Immobilon P (IPVH00010; EMD Millipore). Membrane was blocked in 5% nonfat milk in TBST and incubated with antibodies for Rad21 (H-210; Santa Cruz Biotechnology, Inc.), Smc1a (A300-055A; Bethyl Laboratories, Inc.), Smc3 (ab9263; Abcam), Stag2 (J-12; Santa Cruz Biotechnology, Inc.) and Actin B (C4; EMD Millipore). Secondary antibodies used were HRP conjugated (NA9340 and NA931; GE Healthcare). Blot was visualized using ECL (PI34077 and PI34095; Thermo Fisher Scientific).

**Retrovirus production and infection of c-Kit$^+$ cells.** Virus was produced in 293T cells. Cells were transfected with 20 µg of plasmids using the calcium phosphate protocol. Supernatant containing the virus was harvested 36, 48, and 60 h after transfection. Virus was cleared using a 20-µm filter and concentrated (Amicon Ultra-15, 100 kD MWCO) to ∼1/10 volume. Virus was snap frozen and stored at −80°C. Mouse bone marrow cells were isolated from femur, tibia, and pelvic bones. Cells were blocked with rat IgG (I8015; Sigma-Aldrich) and labeled with CD117-MicroBeads (130-091-224; Miltenyi Biotec) for 15 min at 4°C. Cell suspension was selected on AutoMACS (Miltenyi Biotec), and c-Kit$^+$ cells were seeded at 500,000/ml in Opti-MEM (31985-070; Life Technologies) supplemented with 10% FCS, 55 µM β-mercaptoethanol (21985-023; Gibco), 50 ng/ml SCF (250-03; PeproTech), 50 ng/ml Flt3-Ligand (250-31L; PeproTech), 10 ng/ml IL-3 (213-13; PeproTech), and 10 ng/ml IL-6 (216-16; PeproTech). Virus was added 24 h after cell seeding in growth media with 8 µg/ml polybrene. Viral transduction was monitored 48 h after virus addition by FACS analysis.

**CFU assay.** To address self-renewal capacity, 2,000 retrovirally infected GFP$^+$ or 20,000 total bone marrow cells were seeded in 0.5 ml (per well in 24-well plate) methylcellulose (M3434; STEMCELL Technologies). After 7-d incubation time, GFP$^+$ colonies were counted. FACS analysis was performed to confirm GFP expression and for markers of differentiation. The following antibodies were used at 1/10,000 dilution Cd11b (clone M1/70), Gr1 (clone RB6-8C5), c-Kit (clone 2B8), and Sca-1 (clone D7). For serial replating experiments 2,000 GFP$^+$ cells were seeded as above.

**qRT-PCR.** RNA was isolated using RNeasy mini plus kit (QIAGEN). cDNA was synthesized with a high-capacity RNA-to-cDNA kit (4387406; Life Technologies). The qRT-PCR reaction was performed in a volume of 10 µl with SYBR green (04887352001; Roche) and run on a LightCycler 480 machine (Roche) in 384-well plates. The following qRT-PCR primers (all for mouse) were used in this study: ACTB-F, 5′-GGCTGTATTCCCCTCCATCG-3′; ACTB-R, 5′-CCAGTTGGTAACAATGCCATGT-3′; Rad21-F, 5′-GCCCATGTATTTGAGTGCAA-3′; Rad21-R, 5′-ACTCCCAGGAGAAGGTGTCC-3′; Smc1a-F, 5′-TATCTATGCTCGAGAGGCCC-3′; Smc1a-R, 5′-TTGCTTGATTTCTTCCTCCG-3′; Smc3-F, 5′-TTCCGAAGTTACCGAGACCA-3′; Smc3-R, 5′-GTTGCTTTTTCCAGAGCCA-3′; Stag2-F, 5′-CAGCTGAATGTCATCCTCCC-3′; and Stag2-R, 5′-GCAAACAGCTCAGTGATTCTTG-3′.

**RNA sequencing and analysis.** RNA was isolated using RNeasy mini plus reagents (QIAGEN), and RNA sequencing was performed using the NEXTflex Rapid Directional RNA-Seq kit (5138-07; Bioo Scientific). Libraries were barcoded with NEXTflex adapters and quantified using qPCR and Qubit (Life Technologies). Libraries were sequenced at a HiSeq 2000 (Ilumina). Next, sequencing data analysis was performed as follows. Reads were aligned to mm9 reference genome using TopHat, and Cuffdiff was used to find differentially expressed genes (Trapnell et al., 2012). Heat maps were generated in multiple experiment viewer (MEV; http://www.tm4.org). GSEA was performed by running RNA sequencing data from LSK cells isolated from Renilla$^{(shRNA/+)}$, Smc1a$^{(shRNA/+)}$, and Stag2$^{(shRNA/+)}$ against gene sets for GMP and LT-HSC subtypes that were generated by taking the most differential expressed genes from the Immunological Genome Project (Table S6; Shay and Kang, 2013).

**Metaphase spreads.** Cells were grown in the presence of 0.1 µg/ml nocodazole for 1–4 h. Cells were harvested and resuspended in ice-cold 0.56% KCl. Cells were fixed in ice-cold methanol/glacial acetic acid (3:1) solution and dropped in cold glass slides from circa 50 cm. Slides were air-dried and stained with DAPI. Metaphases were acquired using Metafer (Metasystems) microscope and software.

**shRNA mouse generation and handling.** To generate shRNA mice for cohesin, we tested 10 shRNAs for Rad21, and Smc1a and Stag2 were cloned in the pLMP retroviral backbone. These shRNAs were tested in 3T3 cells for their knockdown efficiency. For each of the targeted genes, one shRNA was chosen that produced knockdown between 75–90%. The selected shRNA sequence was subsequently cloned in the 3′ UTR of a GFP gene downstream of a TRE. TRE, GFP, and shRNA were targeted together to the Col1A1 locus. Targeted ES cells were injected using tetraploid complementation technique. Resulting shRNA mice were bred on a mixed C57BL/6 × 129/SV background. For the majority of experiments, mice used were heterozygous for shRNA and rtTA. To induce shRNA expression, mice were fed chow containing 1 g/kg doxycycline (Bio Serv). Animal care was in accordance with institutional guidelines and approved by the Institutional Animal Care and Use Committee of the New York University School of Medicine.

shRNA sequences as used in shRNA mice in this study are as follows: Rad21-920, 5′-GCTGGCGGTATATTAGATGACAATAGTGAAGCCACAGATGTATTGTCATCTAATATACCGCCAT-3′; Smc1a-3921, 5′-GATGCATGTTAGATTGTTTGCAATAGTGAAGCCACAGATGTATTGCAAACAATCTAACATGCAC-3′; and Stag2-744, 5′-GATCAGAGCATTTCGACATACAATAGTGAAGCCACAGATGTATTGTATGTCGAAATGCTCTGAC-3′.

**FACS analysis.** Peripheral blood was extracted by retroorbital bleeding and blood was collected in EDTA-coated tubes. Red blood cells were lysed with ACK buffer (Quality Biological 118-156-101) for 5 min on ice. Bone marrow was isolated the tibia, femur, and pelvic bones by spinning cleaned bones for 2 min at 8,000 rpm. Single cell suspensions of spleen and thymus were prepared in FACS buffer (3% FBS in PBS) by crushing the organ

through a 70-µm strainer with a plunger. Cells were blocked with rat IgG (I8015; Sigma-Aldrich) for 20 min on ice. Staining for cell surface antigens was performed by adding fluorochrome- or biotin-conjugated antibodies on ice between 20 min and overnight on ice in the dark. The following antibodies were used in this study: anti-CD11b (M1/70), anti–Gr-1 (RB6-8C5), anti-B220 (RA3-6B2), and anti–Sca-1 (D7) all from BD; anti-CD71 (RI7217), anti–Ter-119 (116228), anti–c-Kit (CD117, 2B8), anti-CD150 (TC15-12F12.2), and anti-CD48 (HM481), all from BioLegend; and anti-CD3 (145-2C11) from Thermo Fisher Scientific.

**Histology.** For histological analyses, mouse tissues were fixed in 10% buffered formalin. Fixed tissues were paraffin-embedded, sectioned, and stained with hematoxylin and eosin (H&E) according to standard laboratory protocols.

**Statistical tests and error bars.** All p-values were calculated using unpaired two-tailed Student's *t* test. Statistically significant differences are indicated with asterisks in figures with the accompanying p-value in the legend. Error bars in figures indicate SD for the number of replicates as indicated in the figure legend.

**ATAC-seq.** ATAC sequencing was performed as described earlier (Buenrostro et al., 2015). The resulting library was sequenced in HiSeq2000. Reads were aligned with bowtie on mm9. Peaks were called with PeaKDEck (McCarthy and O'Callaghan, 2014). HTSeq was used to measure count density at peak sites (Anders et al., 2015). Areas with differential accessibility were identified with DESeq2 (Anders and Huber, 2010). GO term biological enrichment was obtained by entering the enriched areas from either Renilla or Stag2 knockdown ATAC-seq in GREAT (McLean et al., 2010). Transcription factor motifs were discovered by entering enriched regions in i-cisTarget (Imrichová et al., 2015).

**Accession numbers for high-throughput sequencing experiments.** Unprocessed and processed data for all high-throughput sequencing experiments in this study can be found in the GEO super series GSE72370: specifically, ATAC sequencing (GSE72367), RNA sequencing in CFU replating cells (GSE72368), and RNA sequencing in LSK cells (GSE72369).

**Online supplemental material.** Table S1, included as a separate Excel file, lists targeting sequences of shRNAs used in retroviral plasmids. Table S2, included as a separate Excel file, lists differentially expressed genes in control (Renilla) and cohesin (Rad21, Smc1a, Smc3, and Stag2) cells from the first (P1) and fifth (P5) plating from the CFU assay; only genes with expression levels of FPKM > 5 are listed. Table S3, included as a separate Excel file, lists differentially expressed genes in control (Renilla) and cohesin (Smc1a and Stag2) knockdown LSK cells sorted from mice treated with doxycycline for 10 d; only genes with expression levels of FPKM > 5 are listed. Table S4, included as a separate Excel file, shows peaks from ATAC sequencing on sorted LSK cells from Renilla and Stag2 shRNA mice treated with doxycycline for 10 d. Table S5, included as a separate Excel file, shows GO factors as found by GREAT analysis of regions that are specifically enriched in $Stag2^{(shRNA/+)}$ LSK cells and GO factors as found by GREAT analysis of regions that are specifically enriched in $Renilla^{(shRNA/+)}$ LSK cells (top 50 are shown for each). Table S6, included as a separate Excel file, shows gene set used to analyze RNA-seq from LSK cells. Online supplemental material is available at http://www.jem.org/cgi/content/full/jem.20151323/DC1.

We would like to thank Peter van Galen and Bradley Bernstein (Broad Institute) for help with the epigenetic mapping in small populations. We also thank the Rodent Genetic Engineering Core (RGEC) for ES cell tetraploid injections (supported in part by grant UL1 TR00038 from the National Center for Advancing Translational Sciences [NCATS], National Institutes of Health), the Immunohistochemistry and Histopathology Core for organ histology, and the Cytometry and Cell Sorting facility (both supported by the Cancer Center Support Grant, P30CA016087). All are at the New York University Langone Medical Center (NYULMC). We thank the NYULMC Genome Technology Center (GTC) for sequencing. This shared resource is partially supported by the Cancer Center Support Grant, P30CA016087, at the Laura and Isaac Perlmutter Cancer Center. This work has used computing resources at the High Performance Computing Facility (HPCF) of the Center for Health Informatics and Bioinformatics at the NYULMC. We thank members of the Aifantis laboratory for helpful discussion.

This research was supported by the US National Institutes of Health (grants 5RO1CA194923, 1R01CA169784, 1R01CA133379, 1R01CA105129, 1R01CA149655 and 5R01CA173636), the William Lawrence and Blanche Hughes Foundation, the Leukemia and Lymphoma Society (TRP#6340-11 and LLS#6373-13), the Chemotherapy Foundation, the V Foundation for Cancer Research, Alex's Lemonade Stand Foundation for Childhood Cancer, St. Baldrick's Cancer Research Foundation, the Dutch Cancer Society (KWF BUIT2012-5358, to J. Mullenders), Deutsche José Carreras Leukämie-Stiftung e.V. (to B. Aranda-Orgilles), and the Howard Hughes Medical Institute (to I. Aifantis).

Prem K. Premsrirut is a founder, officer, and shareholder of Mirimus Inc. The authors declare no additional competing financial interests.

Author contributions: J. Mullenders and I. Aifantis conceived the experiments and analyzed the data and wrote the manuscript. J. Mullenders, K. Wang, and C. Kayembe managed the shRNA mouse colony. J. Mullenders performed in vitro CFU experiments. J. Mullenders and P.P. Rocha performed karyotype analysis. P. Lhoumaud, M. Keller, J. Pae, B. Aranda-Orgilles, P.K. Premsrirut, and L. Cimmino provided technical assistance. B. Aranda-Orgilles, R. Raviram, Y. Gong, and A. Tsirigos provided bioinformatics support. D. Hoehn analyzed the histology of diseased animals. J.A. Skok and R. Bonneau are supervising R. Raviram.

**Submitted: 17 August 2015**
**Accepted: 4 September 2015**

## REFERENCES

Anders, S., and W. Huber. 2010. Differential expression analysis for sequence count data. *Genome Biol*. 11:R106. http://dx.doi.org/10.1186/gb-2010-11-10-r106

Anders, S., P.T. Pyl, and W. Huber. 2015. HTSeq—a Python framework to work with high-throughput sequencing data. *Bioinformatics*. 31:166–169. http://dx.doi.org/10.1093/bioinformatics/btu638

Balbás-Martínez, C., A. Sagrera, E. Carrillo-de-Santa-Pau, J. Earl, M. Márquez, M. Vazquez, E. Lapi, F. Castro-Giner, S. Beltran, M. Bayés, et al. 2013. Recurrent inactivation of STAG2 in bladder cancer is not associated with aneuploidy. *Nat. Genet*. 45:1464–1469. http://dx.doi.org/10.1038/ng.2799

Bolden, J.E., N. Tasdemir, L.E. Dow, J.H. van Es, J.E. Wilkinson, Z. Zhao, H. Clevers, and S.W. Lowe. 2014. Inducible in vivo silencing of Brd4 identifies potential toxicities of sustained BET protein inhibition. *Cell Reports*. 8:1919–1929. http://dx.doi.org/10.1016/j.celrep.2014.08.025

Buenrostro, J.D., B. Wu, H.Y. Chang, and W.J. Greenleaf. 2015. ATAC-seq: A method for assaying chromatin accessibility genome-wide. *Curr. Protoc. Mol. Biol*. 109:1–9. http://dx.doi.org/10.1002/0471142727.mb2129s109

Cancer Genome Atlas Research Network. 2013. Genomic and epigenomic landscapes of adult de novo acute myeloid leukemia. *N. Engl. J. Med*. 368:2059–2074. http://dx.doi.org/10.1056/NEJMoa1301689

Celik, H., C. Mallaney, A. Kothari, E.L. Ostrander, E. Eultgen, A. Martens, C.A. Miller, J. Hundal, J.M. Klco, and G.A. Challen. 2015. Enforced differentiation of Dnmt3a-null bone marrow leads to failure with c-Kit mutations driving leukemic transformation. *Blood*. 125:619–628. http://dx.doi.org/10.1182/blood-2014-08-594564

Chu, S.H., D. Heiser, L. Li, I. Kaplan, M. Collector, D. Huso, S.J. Sharkis, C. Civin, and D. Small. 2012. FLT3-ITD knockin impairs hematopoietic stem cell quiescence/homeostasis, leading to myeloproliferative neoplasm. *Cell Stem Cell*. 11:346–358. http://dx.doi.org/10.1016/j.stem.2012.05.027

Crispino, J.D. 2005. GATA1 in normal and malignant hematopoiesis. *Semin. Cell Dev. Biol*. 16:137–147. http://dx.doi.org/10.1016/j.semcdb.2004.11.002

Crompton, B.D., C. Stewart, A. Taylor-Weiner, G. Alexe, K.C. Kurek, M.L. Calicchio, A. Kiezun, S.L. Carter, S.A. Shukla, S.S. Mehta, et al. 2014. The genomic landscape of pediatric Ewing sarcoma. *Cancer Discov*. 4:1326–1341. http://dx.doi.org/10.1158/2159-8290.CD-13-1037

Ding, L., T.J. Ley, D.E. Larson, C.A. Miller, D.C. Koboldt, J.S. Welch, J.K. Ritchey, M.A. Young, T. Lamprecht, M.D. McLellan, et al. 2012. Clonal evolution in relapsed acute myeloid leukaemia revealed by whole-genome sequencing. *Nature*. 481:506–510. http://dx.doi.org/10.1038/nature10738

Dixon, J.R., S. Selvaraj, F. Yue, A. Kim, Y. Li, Y. Shen, M. Hu, J.S. Liu, and B. Ren. 2012. Topological domains in mammalian genomes identified by analysis of chromatin interactions. *Nature*. 485:376–380. http://dx.doi.org/10.1038/nature11082

Dowen, J.M., Z.P. Fan, D. Hnisz, G. Ren, B.J. Abraham, L.N. Zhang, A.S. Weintraub, J. Schuijers, T.I. Lee, K. Zhao, and R.A. Young. 2014. Control of cell identity genes occurs in insulated neighborhoods in mammalian chromosomes. *Cell*. 159:374–387. http://dx.doi.org/10.1016/j.cell.2014.09.030

Genovese, G., A.K. Kähler, R.E. Handsaker, J. Lindberg, S.A. Rose, S.F. Bakhoum, K. Chambert, E. Mick, B.M. Neale, M. Fromer, et al. 2014. Clonal hematopoiesis and blood-cancer risk inferred from blood DNA sequence. *N. Engl. J. Med*. 371:2477–2487. http://dx.doi.org/10.1056/NEJMoa1409405

Gruber, S., C.H. Haering, and K. Nasmyth. 2003. Chromosomal cohesin forms a ring. *Cell*. 112:765–777. http://dx.doi.org/10.1016/S0092-8674(03)00162-4

Guo, G., X. Sun, C. Chen, S. Wu, P. Huang, Z. Li, M. Dean, Y. Huang, W. Jia, Q. Zhou, et al. 2013. Whole-genome and whole-exome sequencing of bladder cancer identifies frequent alterations in genes involved in sister chromatid cohesion and segregation. *Nat. Genet*. 45:1459–1463. http://dx.doi.org/10.1038/ng.2798

Haarhuis, J.H., A.M. Elbatsh, and B.D. Rowland. 2014. Cohesin and its regulation: on the logic of X-shaped chromosomes. *Dev. Cell*. 31:7–18. http://dx.doi.org/10.1016/j.devcel.2014.09.010

Hauf, S., E. Roitinger, B. Koch, C.M. Dittrich, K. Mechtler, and J.M. Peters. 2005. Dissociation of cohesin from chromosome arms and loss of arm cohesion during early mitosis depends on phosphorylation of SA2. *PLoS Biol*. 3:e69. http://dx.doi.org/10.1371/journal.pbio.0030069

Hirano, T. 2005. SMC proteins and chromosome mechanics: from bacteria to humans. *Philos. Trans. R. Soc. Lond. B Biol. Sci*. 360:507–514. http://dx.doi.org/10.1098/rstb.2004.1606

Holwerda, S., and W. de Laat. 2012. Chromatin loops, gene positioning, and gene expression. *Front. Genet*. 3:217. http://dx.doi.org/10.3389/fgene.2012.00217

Hoque, M.T., and F. Ishikawa. 2002. Cohesin defects lead to premature sister chromatid separation, kinetochore dysfunction, and spindle-assembly checkpoint activation. *J. Biol. Chem*. 277:42306–42314. http://dx.doi.org/10.1074/jbc.M206836200

Huether, R., L. Dong, X. Chen, G. Wu, M. Parker, L. Wei, J. Ma, M.N. Edmonson, E.K. Hedlund, M.C. Rusch, et al. 2014. The landscape of somatic mutations in epigenetic regulators across 1,000 paediatric cancer genomes. *Nat. Commun*. 5:3630. http://dx.doi.org/10.1038/ncomms4630

Imrichová, H., G. Hulselmans, Z.K. Atak, D. Potier, and S. Aerts. 2015. i-cisTarget 2015 update: generalized cis-regulatory enrichment analysis in human, mouse and fly. *Nucleic Acids Res*. 43:W57–W64. http://dx.doi.org/10.1093/nar/gkv395

Jan, M., T.M. Snyder, M.R. Corces-Zimmerman, P. Vyas, I.L. Weissman, S.R. Quake, and R. Majeti. 2012. Clonal evolution of preleukemic hematopoietic stem cells precedes human acute myeloid leukemia. *Sci. Transl. Med*. 4:149ra118. http://dx.doi.org/10.1126/scitranslmed.3004315

Kagey, M.H., J.J. Newman, S. Bilodeau, Y. Zhan, D.A. Orlando, N.L. van Berkum, C.C. Ebmeier, J. Goossens, P.B. Rahl, S.S. Levine, et al. 2010. Mediator and cohesin connect gene expression and chromatin architecture. *Nature*. 467:430–435. http://dx.doi.org/10.1038/nature09380

Kon, A., L.Y. Shih, M. Minamino, M. Sanada, Y. Shiraishi, Y. Nagata, K. Yoshida, Y. Okuno, M. Bando, R. Nakato, et al. 2013. Recurrent mutations in multiple components of the cohesin complex in myeloid neoplasms. *Nat. Genet*. 45:1232–1237. http://dx.doi.org/10.1038/ng.2731

Laugsch, M., J. Seebach, H. Schnittler, and R. Jessberger. 2013. Imbalance of SMC1 and SMC3 cohesins causes specific and distinct effects. *PLoS ONE*. 8:e65149. http://dx.doi.org/10.1371/journal.pone.0065149

Lee, B.H., Z. Tothova, R.L. Levine, K. Anderson, N. Buza-Vidas, D.E. Cullen, E.P. McDowell, J. Adelsperger, S. Fröhling, B.J. Huntly, et al. 2007. FLT3 mutations confer enhanced proliferation and survival properties to multipotent progenitors in a murine model of chronic myelomonocytic leukemia. *Cancer Cell*. 12:367–380. http://dx.doi.org/10.1016/j.ccr.2007.08.031

Leiserson, M.D., F. Vandin, H.T. Wu, J.R. Dobson, J.V. Eldridge, J.L. Thomas, A. Papoutsaki, Y. Kim, B. Niu, M. McLellan, et al. 2015. Pan-cancer network analysis identifies combinations of rare somatic mutations across pathways and protein complexes. *Nat. Genet*. 47:106–114. http://dx.doi.org/10.1038/ng.3168

Li, X., T.W. Zhang, J.L. Tang, P.P. Fa, J.X. Lu, F.M. Qi, Z.M. Cai, C.X. Liu, and X.J. Sun. 2015. Loss of STAG2 causes aneuploidy in normal human bladder cells. *Genet. Mol. Res*. 14:2638–2646. http://dx.doi.org/10.4238/2015.March.30.24

Lieberman-Aiden, E., N.L. van Berkum, L. Williams, M. Imakaev, T. Ragoczy, A. Telling, I. Amit, B.R. Lajoie, P.J. Sabo, M.O. Dorschner, et al. 2009. Comprehensive mapping of long-range interactions reveals folding principles of the human genome. *Science*. 326:289–293. http://dx.doi.org/10.1126/science.1181369

Lindsley, R.C., B.G. Mar, E. Mazzola, P.V. Grauman, S. Shareef, S.L. Allen, A. Pigneux, M. Wetzler, R.K. Stuart, H.P. Erba, et al. 2015. Acute myeloid leukemia ontogeny is defined by distinct somatic mutations. *Blood*. 125:1367–1376. http://dx.doi.org/10.1182/blood-2014-11-610543

Mannini, L., F. Cucco, V. Quarantotti, I.D. Krantz, and A. Musio. 2013. Mutation spectrum and genotype-phenotype correlation in Cornelia de Lange syndrome. *Hum. Mutat*. 34:1589–1596. http://dx.doi.org/10.1002/humu.22430

McCarthy, M.T., and C.A. O'Callaghan. 2014. PeaKDEck: a kernel density estimator-based peak calling program for DNaseI-seq data. *Bioinformatics*. 30:1302–1304. http://dx.doi.org/10.1093/bioinformatics/btt774

McLean, C.Y., D. Bristor, M. Hiller, S.L. Clarke, B.T. Schaar, C.B. Lowe, A.M. Wenger, and G. Bejerano. 2010. GREAT improves functional interpretation of cis-regulatory regions. *Nat. Biotechnol*. 28:495–501. http://dx.doi.org/10.1038/nbt.1630

Mizuguchi, T., G. Fudenberg, S. Mehta, J.M. Belton, N. Taneja, H.D. Folco, P. FitzGerald, J. Dekker, L. Mirny, J. Barrowman, and S.I. Grewal. 2014. Cohesin-dependent globules and heterochromatin shape 3D genome architecture in S. pombe. *Nature*. 516:432–435. http://dx.doi.org/10.1038/nature13833

Moran-Crusio, K., L. Reavie, A. Shih, O. Abdel-Wahab, D. Ndiaye-Lobry, C. Lobry, M.E. Figueroa, A. Vasanthakumar, J. Patel, X. Zhao, et al. 2011. Tet2 loss leads to increased hematopoietic stem cell self-renewal and myeloid transformation. *Cancer Cell*. 20:11–24. http://dx.doi.org/10.1016/j.ccr.2011.06.001

Nasmyth, K., and C.H. Haering. 2009. Cohesin: its roles and mechanisms. *Annu. Rev. Genet*. 43:525–558. http://dx.doi.org/10.1146/annurev-genet-102108-134233

Nikolaev, S.I., F. Santoni, A. Vannier, E. Falconnet, E. Giarin, G. Basso, A. Hoischen, J.A. Veltman, J. Groet, D. Nizetic, and S.E. Antonarakis. 2013. Exome sequencing identifies putative drivers of progression of transient myeloproliferative disorder to AMKL in infants with Down syndrome. *Blood*. 122:554–561. http://dx.doi.org/10.1182/blood-2013-03-491936

Parelho, V., S. Hadjur, M. Spivakov, M. Leleu, S. Sauer, H.C. Gregson, A. Jarmuz, C. Canzonetta, Z. Webster, T. Nesterova, et al. 2008. Cohesins functionally associate with CTCF on mammalian chromosome arms. *Cell*. 132:422–433. http://dx.doi.org/10.1016/j.cell.2008.01.011

Phillips-Cremins, J.E., M.E. Sauria, A. Sanyal, T.I. Gerasimova, B.R. Lajoie, J.S. Bell, C.T. Ong, T.A. Hookway, C. Guo, Y. Sun, et al. 2013. Architectural protein subclasses shape 3D organization of genomes during lineage commitment. *Cell*. 153:1281–1295.

Premsrirut, P.K., L.E. Dow, S.Y. Kim, M. Camiolo, C.D. Malone, C. Miething, C. Scuoppo, J. Zuber, R.A. Dickins, S.C. Kogan, et al. 2011. A rapid and scalable system for studying gene function in mice using conditional RNA interference. *Cell*. 145:145–158. http://dx.doi.org/10.1016/j.cell.2011.03.012

Quivoron, C., L. Couronné, V. Della Valle, C.K. Lopez, I. Plo, O. Wagner-Ballon, M. Do Cruzeiro, F. Delhommeau, B. Arnulf, M.H. Stern, et al.

2011. TET2 inactivation results in pleiotropic hematopoietic abnormalities in mouse and is a recurrent event during human lymphomagenesis. *Cancer Cell*. 20:25–38. http://dx.doi.org/10.1016/j.ccr.2011.06.003

Rickman, D.S., T.D. Soong, B. Moss, J.M. Mosquera, J. Dlabal, S. Terry, T.Y. MacDonald, J. Tripodi, K. Bunting, V. Najfeld, et al. 2012. Oncogene-mediated alterations in chromatin conformation. *Proc. Natl. Acad. Sci. USA*. 109:9083–9088. http://dx.doi.org/10.1073/pnas.1112570109

Rocquain, J., V. Gelsi-Boyer, J. Adélaïde, A. Murati, N. Carbuccia, N. Vey, D. Birnbaum, M.J. Mozziconacci, and M. Chaffanet. 2010. Alteration of cohesin genes in myeloid diseases. *Am. J. Hematol.* 85:717–719. http://dx.doi.org/10.1002/ajh.21798

Seitan, V.C., B. Hao, K. Tachibana-Konwalski, T. Lavagnolli, H. Mira-Bontenbal, K.E. Brown, G. Teng, T. Carroll, A. Terry, K. Horan, et al. 2011. A role for cohesin in T-cell-receptor rearrangement and thymocyte differentiation. *Nature*. 476:467–471. http://dx.doi.org/10.1038/nature10312

Seitan, V.C., A.J. Faure, Y. Zhan, R.P. McCord, B.R. Lajoie, E. Ing-Simmons, B. Lenhard, L. Giorgetti, E. Heard, A.G. Fisher, et al. 2013. Cohesin-based chromatin interactions enable regulated gene expression within preexisting architectural compartments. *Genome Res.* 23:2066–2077. http://dx.doi.org/10.1101/gr.161620.113

Shay, T., and J. Kang. 2013. Immunological Genome Project and systems immunology. *Trends Immunol.* 34:602–609. http://dx.doi.org/10.1016/j.it.2013.03.004

Shlush, L.I., S. Zandi, A. Mitchell, W.C. Chen, J.M. Brandwein, V. Gupta, J.A. Kennedy, A.D. Schimmer, A.C. Schuh, K.W. Yee, et al. HALT Pan-Leukemia Gene Panel Consortium. 2014. Identification of pre-leukaemic haematopoietic stem cells in acute leukaemia. *Nature*. 506:328–333. (published erratum appears in Nature. 2014. 508:420) http://dx.doi.org/10.1038/nature13038

Sofueva, S., E. Yaffe, W.C. Chan, D. Georgopoulou, M. Vietri Rudan, H. Mira-Bontenbal, S.M. Pollard, G.P. Schroth, A. Tanay, and S. Hadjur. 2013. Cohesin-mediated interactions organize chromosomal domain architecture. *EMBO J.* 32:3119–3129. http://dx.doi.org/10.1038/emboj.2013.237

Solomon, D.A., T. Kim, L.A. Diaz-Martinez, J. Fair, A.G. Elkahloun, B.T. Harris, J.A. Toretsky, S.A. Rosenberg, N. Shukla, M. Ladanyi, et al. 2011. Mutational inactivation of STAG2 causes aneuploidy in human cancer. *Science*. 333:1039–1043. http://dx.doi.org/10.1126/science.1203619

Solomon, D.A., J.S. Kim, J. Bondaruk, S.F. Shariat, Z.F. Wang, A.G. Elkahloun, T. Ozawa, J. Gerard, D. Zhuang, S. Zhang, et al. 2013. Frequent truncating mutations of STAG2 in bladder cancer. *Nat. Genet.* 45:1428–1430. http://dx.doi.org/10.1038/ng.2800

Takiguchi, M., L.E. Dow, J.E. Prier, C.L. Carmichael, B.T. Kile, S.J. Turner, S.W. Lowe, D.C. Huang, and R.A. Dickins. 2013. Variability of inducible expression across the hematopoietic system of tetracycline transactivator transgenic mice. *PLoS ONE*. 8:e54009. http://dx.doi.org/10.1371/journal.pone.0054009

Thol, F., R. Bollin, M. Gehlhaar, C. Walter, M. Dugas, K.J. Suchanek, A. Kirchner, L. Huang, A. Chaturvedi, M. Wichmann, et al. 2014. Mutations in the cohesin complex in acute myeloid leukemia: clinical and prognostic implications. *Blood*. 123:914–920. http://dx.doi.org/10.1182/blood-2013-07-518746

Thota, S., A.D. Viny, H. Makishima, B. Spitzer, T. Radivoyevitch, B. Przychodzen, M.A. Sekeres, R.L. Levine, and J.P. Maciejewski. 2014. Genetic alterations of the cohesin complex genes in myeloid malignancies. *Blood*. 124:1790–1798. http://dx.doi.org/10.1182/blood-2014-04-567057

Tirode, F., D. Surdez, X. Ma, M. Parker, M.C. Le Deley, A. Bahrami, Z. Zhang, E. Lapouble, S. Grossetête-Lalami, M. Rusch, et al. St. Jude Children's Research Hospital–Washington University Pediatric Cancer Genome Project and the International Cancer Genome Consortium. 2014. Genomic landscape of Ewing sarcoma defines an aggressive subtype with co-association of STAG2 and TP53 mutations. *Cancer Discov.* 4:1342–1353. http://dx.doi.org/10.1158/2159-8290.CD-14-0622

Trapnell, C., A. Roberts, L. Goff, G. Pertea, D. Kim, D.R. Kelley, H. Pimentel, S.L. Salzberg, J.L. Rinn, and L. Pachter. 2012. Differential gene and transcript expression analysis of RNA-seq experiments with TopHat and Cufflinks. *Nat. Protoc.* 7:562–578. http://dx.doi.org/10.1038/nprot.2012.016

Vass, S., S. Cotterill, A.M. Valdeolmillos, J.L. Barbero, E. Lin, W.D. Warren, and M.M. Heck. 2003. Depletion of Drad21/Scc1 in *Drosophila* cells leads to instability of the cohesin complex and disruption of mitotic progression. *Curr. Biol.* 13:208–218. http://dx.doi.org/10.1016/S0960-9822(03)00047-2

Viny, A.D., C.J. Ott, B. Spitzer, M. Rivas, C. Meydan, E. Papalexi, D. Yelin, K. Shank, J. Reyes, A. Chiu, et al. 2015. Dose-dependent role of the cohesin complex in normal and malignant hematopoiesis. *J. Exp. Med.* 212. http://dx.doi.org/10.1084/jem.20151317

Waizenegger, I.C., S. Hauf, A. Meinke, and J.M. Peters. 2000. Two distinct pathways remove mammalian cohesin from chromosome arms in prophase and from centromeres in anaphase. *Cell*. 103:399–410. http://dx.doi.org/10.1016/S0092-8674(00)00132-X

Watrin, E., and J.M. Peters. 2006. Cohesin and DNA damage repair. *Exp. Cell Res.* 312:2687–2693. http://dx.doi.org/10.1016/j.yexcr.2006.06.024

Wendt, K.S., K. Yoshida, T. Itoh, M. Bando, B. Koch, E. Schirghuber, S. Tsutsumi, G. Nagae, K. Ishihara, T. Mishiro, et al. 2008. Cohesin mediates transcriptional insulation by CCCTC-binding factor. *Nature*. 451:796–801. http://dx.doi.org/10.1038/nature06634

Xu, H., K. Balakrishnan, J. Malaterre, M. Beasley, Y. Yan, J. Essers, E. Appeldoorn, J.M. Tomaszewski, M. Vazquez, S. Verschoor, et al. 2010. Rad21-cohesin haploinsufficiency impedes DNA repair and enhances gastrointestinal radiosensitivity in mice. *PLoS ONE*. 5:e12112. (published erratum appears in PLoS One. 5:http://dx.doi.org/10.1371/annotation/12224797-353c-4e9c-92f3-a0de9b527415) http://dx.doi.org/10.1371/journal.pone.0012112

Yan, J., M. Enge, T. Whitington, K. Dave, J. Liu, I. Sur, B. Schmierer, A. Jolma, T. Kivioja, M. Taipale, and J. Taipale. 2013. Transcription factor binding in human cells occurs in dense clusters formed around cohesin anchor sites. *Cell*. 154:801–813. http://dx.doi.org/10.1016/j.cell.2013.07.034

Yoshida, K., T. Toki, Y. Okuno, R. Kanezaki, Y. Shiraishi, A. Sato-Otsubo, M. Sanada, M.J. Park, K. Terui, H. Suzuki, et al. 2013. The landscape of somatic mutations in Down syndrome-related myeloid disorders. *Nat. Genet.* 45:1293–1299. http://dx.doi.org/10.1038/ng.2759

Zhang, N., Y. Jiang, Q. Mao, B. Demeler, Y.J. Tao, and D. Pati. 2013. Characterization of the interaction between the cohesin subunits Rad21 and SA1/2. *PLoS ONE*. 8:e69458. http://dx.doi.org/10.1371/journal.pone.0069458